ADDIS ABABA UNIVERSITY
SCHOOL OF GRADUATE STUDIES
FACULTY OF SCIENCE
DEPARTMENT OF EARTH SCIENCE

VELOCITY STRUCTURE OF THE UPPER CRUST BENEATH THE NORTHERN MAIN ETHIOPIAN RIFT

Ethiopia Afar Geoscientific
Lithospheric Experiment
2001 - 2003

A THESIS SUBMITTED TO THE SCHOOL OF GRADUATE STUDIES OF ADDIS ABABA UNIVERSITY IN PARTIAL FULFILLMENT OF THE REQUIREMENTS FOR THE DEGREE OF MASTER OF SCIENCE IN GEOPHYSICS

BY: GENNETU KASSIE
JUNE 2005

ACKNOWLEDGMENTS

I am very grateful and indebted to my advisor Dr. Tilahun Mammo for his guidance, support, and cooperation through out the work. The expertise and full confidence of him helped me to complete the work on time with expected result.

I would like also to acknowledge all the staff members of Geophysics department in the Ethiopian Geological Survey. A special thanks is for Ato Befkadu Oluma who is the director of Geophysics department for his extensive material as well as advice support, for Ato Kimemu Nurie, and for Ato Tesfaye Temtmie too. And I also give thanks for the department secretarys Wosenie and Bogalech who are helped me in writing the first copy of this material.

I would also like to give special thanks to my brother Abayneh Kassie and his wife Kidist Alemu together with Eskinder Alemu for their financial support and considerable suggestions and encouragements through out my work.

I would also like to thank Dr. Worasuh Getahune, my classmates Demsachew Abebe, Fissha Ayele, Minilik Wobie, and Yirgalem Negash; and Ato Ali Ahmed and Ato Tesfaye Hailu for their cooperativeness and supportiveness in all aspects in the way of my work.

I would like to thank my family, for their many unselfish sacrifices, which helped me to get an education that has made all the difference, my mother Wobalem Mengistu, my father Kassie Tegegne, my brothers Melaku Tegegne with his wife Tigist, Mulatu Arega, Yitayih Kassie, Zemene Kassie, and Eyob Tollossa; my sisters Abebaye Kassie, Yirbebu Kassie, and Tigist Demelash; and my uncles Demelash Tebikew, Semeineh Mengistu with his wife Aynalem. Their support both morally and financially till the last minutes of the work helped me to complete the work.

Finally, I thank my wife Ethiopia Arega for her understanding and tolerance of my resolve to accomplish this work, and above her loyal support, constant encouragements and welcome practical suggestions.

This work is dedicated to my mother Wobalem Mengistu, my father Kassie Tegegne, my sister Abebaye Kassie, and my wife Ethiopia Arega.

TABLE OF CONTENTS

LIST OF FIGURES:

LIST OF TABLES:

ABSTRACT

Seismic and geologic sections are of the vital importance to the various professional bodies, institutions and industries. They give us an insight on the grounds we are literally standing on. This study has conducted the surface imaging of the earth to a depth of 10 km on a 92.5 km long seismic profile line. The study was conducted starting from the northern most of the Main Ethiopian Rift to the southern most of Afar to give us results, which are archetype to the study area.

For the generation of seismic waves explosives were detonated inside boreholes and programmable seismic energy recorders called "Texans" were deployed on the surface at about one kilometer spacing.

Reduced first arrival P-waves were picked and converted to actual time prior to inversion. The geo-seismic model was inverted by the methods of Generalized Reciprocal Method (GRM).

Four layers at an average depth of 2 km, 4.5 km, and 8.5 km were identified with corresponding average P-wave velocities of 2875 m/s, 4000 m/s, 5700m/s, and 6400 m/s respectively. The geological section of the studied area has been identified to rest on a crystalline basement overlain by Meta-sediments and Meta-volcanic rocks. The first layer has been identified as Miocene-quaternary sediments; Cenozoic volcanic flows.

1. INTRODUCTION

The East African System is one of the most spectacular geologic features of the world. This geologic environment offers a unique opportunity to observe the way in which it is rifting is in accordance with the plate tectonic theory.

The geology and structures of the Main Ethiopian Rift is totally controlled by the rifting process. The aim of this thesis is to map the P-wave velocity distribution of the layers in the upper most crust.

1.1. Previous works

Many geophysical *(seismic)* works were done as the part of the EAGLE project in the year 2004, some of these are:

Evidence for crustal structure influence on the evolution of the Main Ethiopian Rift (*G.D. Mackenzie, et. al., 2004*); EAGLE - The controlled source seismic project *(Magurie, P.K, H, Amha, M., Asfaw, L., Mammo, T., 2004);* A preliminary analysis of crustal structure variation along the Main Ethiopian Rift *(G. Randy Keller et. al.., 2004*); 3D seismic imaging of a proto-ridge axis in the Main Ethiopian Rift *(K. Keranen, et. al.., 2004);* Deep seismic soundings in the Afar region *(Berckhemer et al.. , 1975; Ruegg, 1975);* Velocity structure of the upper most crust across the Main Ethiopian Rift *(Mehari, 2004);*and others.

In regard to geology some works have been reported *(Mohr, 1961; Jusentin, 1974; Kazmin & 1978; Girmay & Assefa, 1989; Boccaletti and Assefa, 1975; Mazzarini & Abebe, 1999; Wolde, 1996, and others).*

1.2. Physiographic outlines

The region described in this study starts from northern most of the Main Ethiopian Rift to the southern most of Afar depression along the Eastern African Rift.

The study area starts at a place called Doni with an elevation of 1236 m, Easting 594590, Northing 976028 and UTM zone 37P to a place called Melke-Sedi with an elevation of 898 m Easting 679730, Northing 1129583 and UTM zone 37P.

1.3. Aim of the present study

The major objectives of this work are:

1) Mapping the seismic layers beneath the northern part of the Main Ethiopian Rift alo the EAGLE profile 2.

2) Interpret the geology.

3) Identify structures if any.

1.4. Methodology

Refraction seismic method has been employed to produce the seismic model beneath the Main Ethiopian Rift. The generalized reciprocal method (GRM) was used to analyze the data and invert the Geo-seismic model.

This seismic model was then interpreted in terms of geology using deterministic P-wave velocities, field investigation to correlate the results obtained in this work with that of the outcrops in the profile and previous regional geological works.

2. REGIONAL GEOLOGY

2.1 Introduction

The geology of the study area is mainly controlled by activities, which control the geology of the country. These geologic activities are, the formation of the Precambrian basement and associated deformation, the deposition of Mesozoic sedimentary succession, the uplifting- volcanism and rifting of the Cenozoic and much more recently the quaternary climate variation and associated lake level changes. All these geologic activities leave their imprint in the geology of the study area.

The Cenozoic uplift and associated rifting have been associated with volcanic activity. This activity leads to the eruption of volcanic rocks such as basalts (the older trap series basalt and the much more recent basaltic scoria cons), ignimbrite, trachyte, rhyolite, and pumiceous and pyroclastic. The faulting also formed structural depressions and calderas, which are later, filled by lakes. The lakes occupied a wide area in the quaternary before they shrunk to the present day size due to climate change. The shrinking lakes left behind latchstring sediments that cover the low-lying plain. Nevertheless, the dominant rocks in the study area are volcanic products of the Cenozoic and the quaternary to recent fluvio-lacustrine sediments.

2.2. The Paleozoic

The Paleozoic extends from the Cambrian to the Permian, during this period, the whole of the Arabo- Ethiopian massif formed a stable landmass subject to denudation resulting in near peneplanation of the ancient pre-Cambrian orogenic mountain ranges at the end of the era. However, some doubtful local occurrences of the Paleozoic strata are worthy of note *(Mohr 1971).*

In the Paleozoic era, two lithological units are discernable, the edaga arbi glacials and the enticho sandstones. It has been noted that the unconformity between the Adigrat sandstone and underlying clastics is not significant. This shows that differentiation between the clastics of the Paleozoic and the Adigrat sandstones of the Mesozoic is barely possible.

2.3. The Mesozoic

Early in the Mesozoic the horn of Africa was marked by the first major transgression of the sea since the end of the pre-Cambrian. The epeirogenic sinking which carried this massive transgression over parts of the ancient continent of the Gondwanaland commenced in Triassic. It reached its maximum development in the early upper Jurassic, after which regression due to eperogenic uplift followed by the end of the Mesozoic almost the entire horn of Africa was again raised above sea level *(V. Kazmin A.A., 1972).*

2.3.1. The Adigrat sandstone

This is a transgressive facies ranging from the upper Triassic age in the Ogaden to lower or possibly even middle Jurassic in Tigray and Eritrea. Induction therefore is that the sea advanced from the SE to the NW.

Whilst in a given part of Ethiopia the thickness of the Adigrat sandstone remains fairly constant, local variations are observed where irregularities in the basement complex peneplain occur. General figure of the central Ethiopia can be given as 500m, but variations in the thickness of the Adigrat sandstone are known as much as 1000m and to as little as a few meters.

The Adigrat sandstone is generally massive and thick bedded. It generally comprises approximately 6/5 major lithologies where the thickness of one may range from maximum of 400m to less than 3m. In the Cherecher (Arussi) highlands the basal Adigrat sandstone formation underling the Jurassic limestone varies in thickness form 200m in the Galleti valley in the SW to only 25m in the Ramis valley in the NE *(V.Kazmin A.A., 1972).*

2.3.2. The Antalo limestone facies

The Antalo limestone has been observed to be lying directly on the basement complex in northern or central Ethiopia, always being underlain by the Adigrat sandstone.

The Antalo limestone comprises many lithological types of limestone and includes layers of marl and silt. The Antalo limestone formation varies in thickness from 0 to 800m. In the Arussi highlands, the Mesozoic succession is up to 1000m.

In Chercher these occur 250m to 460m of limestone resting on the 150m thick Adigrat sandstone formations. However, to the NE, this basal sandstone facies thins out until the limestone occurs resting directly on basement complex rocks *(Mohr, 1971).*

2.3.3. The regressive upper sandstone facies and rocks of cretaceous age.

A new transgression began in the Aptian and this was also the time of a wide spread marine transgression in the whole Middle East. It is important that the first manifestation of basaltic volcanism coincides with the lower cretaceous transgression (tuffs and flows) in the Ambaradam formation *(Abate et al 1969).*

In the Chercher highlands the upper sandstone occurred in irregularly distributed isolated outcrops. In the Soca valley 150m of upper sandstone is typically developed *(Mohr 1997).*

2.4. The Cenozoic

In early Cenozoic extrusion of flood lava occurred from fissures and centers and covered the great part of the Mesozoic sedimentary rocks. According to Zenettin & Justin – Visentin *(1974)* out crops of the Ashangi Basalts (Eocene-Paleocene), consists predominantly of thick basalt lava flow trachytes and rhyolites with inter bedded pyroclastics erupted from fissures. Dolerite sills, acidic dikes, and gabbro-diabase intrusions inject them. The flows have variable thickness of 200-1200m. The thickest exposed sections occur close to the rift escarpment, suggesting that the main source was associated with the rifting.

Magdala group (Upper Pliocene) Outcropped within Ethiopian rift, on the escarpment and near by plateaus. The thickness of the unit increases away from the rift (Morton, et al 1980). Acidic rocks dominate including acid tuffs, mostly ignimbrites, pantelleritic rhyolites and trachytes. They are interbedded with lavas and agglomerates of basaltic composition.

Aden volcanic series rocks postdate the formation of the rift system in Ethiopia, i.e. post Miocene or Plio-Quaternary. Most of the rocks are confined to the rift system and unique out crop on the NW plateau is found south of lake Tana. There is two-fold division if the lavas of the Aden volcanic series, an earlier alkaline-silicis series followed by scoraceos flood basalts.

From late Miocene to Pliocene, volcanism was largely restricted to the rifts. But in some areas they cover the escarpments and even the adjacent plateaux *(Kazmin 1972)*.

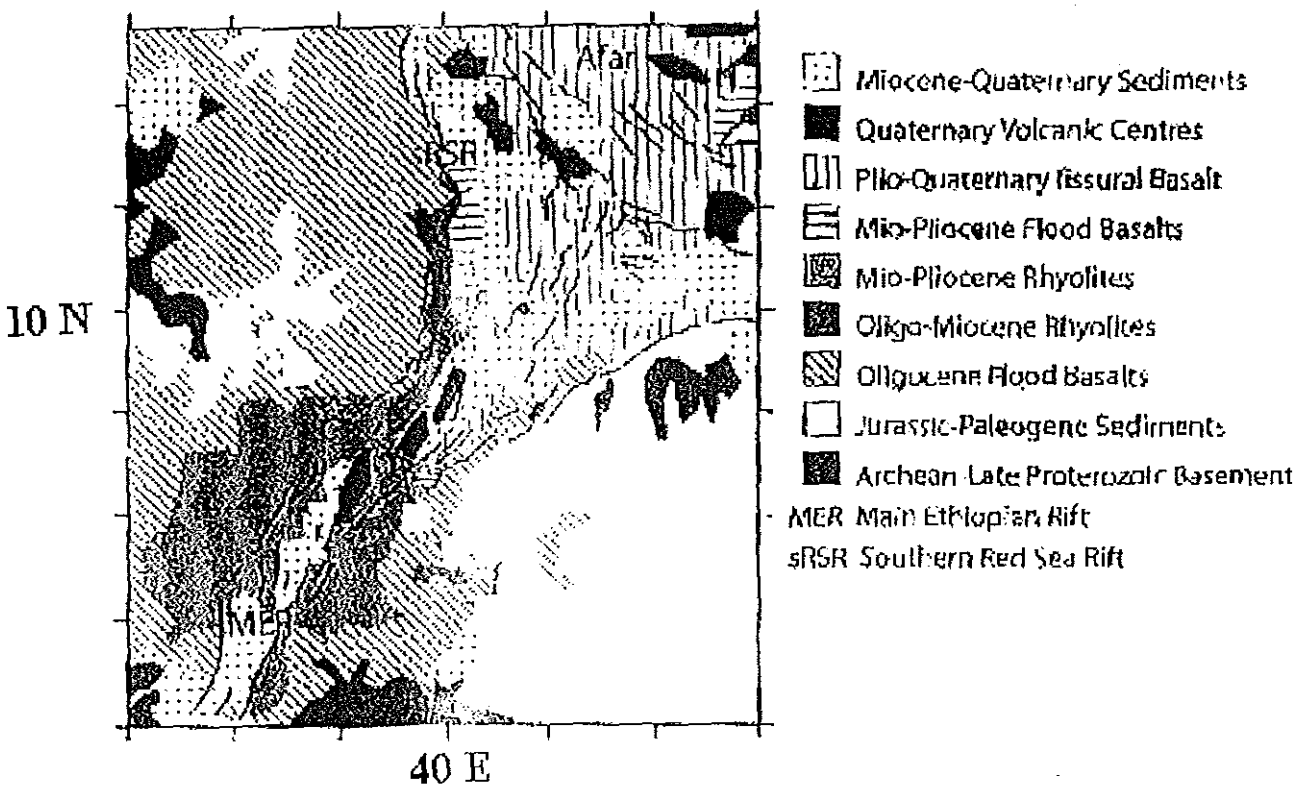

Fig. 2.1. A simplified Geological map of the study area (modified from Wolfenden)

3. PROJECT EAGLE

3.1. Introduction

The Ethiopia Afar Geoscientific Lithospheric Experiment (EAGLE) is a major initiative to investigate how the African continent is splitting along the Ethiopian rift in the horn of Africa. The project involves the universities of Leicester, Leeds, and Royal Holloway from the United Kingdom, Stanford University in California and the University of Texas at El Paso both from the United States. These groups are working with major groups from the Geophysical Observatory and the Department of the Ethiopian Ministry of Mines. The commission of Science and Technology of Democratic Federal Republic of Ethiopia coordinated the whole project.

The project included the carrying out of two seismic profiles; the first, profile 1, across the Ethiopian rift in the vicinity of Nazareth extending to the Blue Nile in NW and to Ginir (in Bale region) in the south east; the second, profile 2, extended along the rift from Awassa in the south to Gewane in the north. A dense network of instruments (profile3) was also to be deployed around the intersection of the two profiles to provide a 3-D tomographic image of the subsurface immediately beneath the neo-volcanic segment of Bosetti in the vicinity of Nazareth *(Fig 3.1)*.

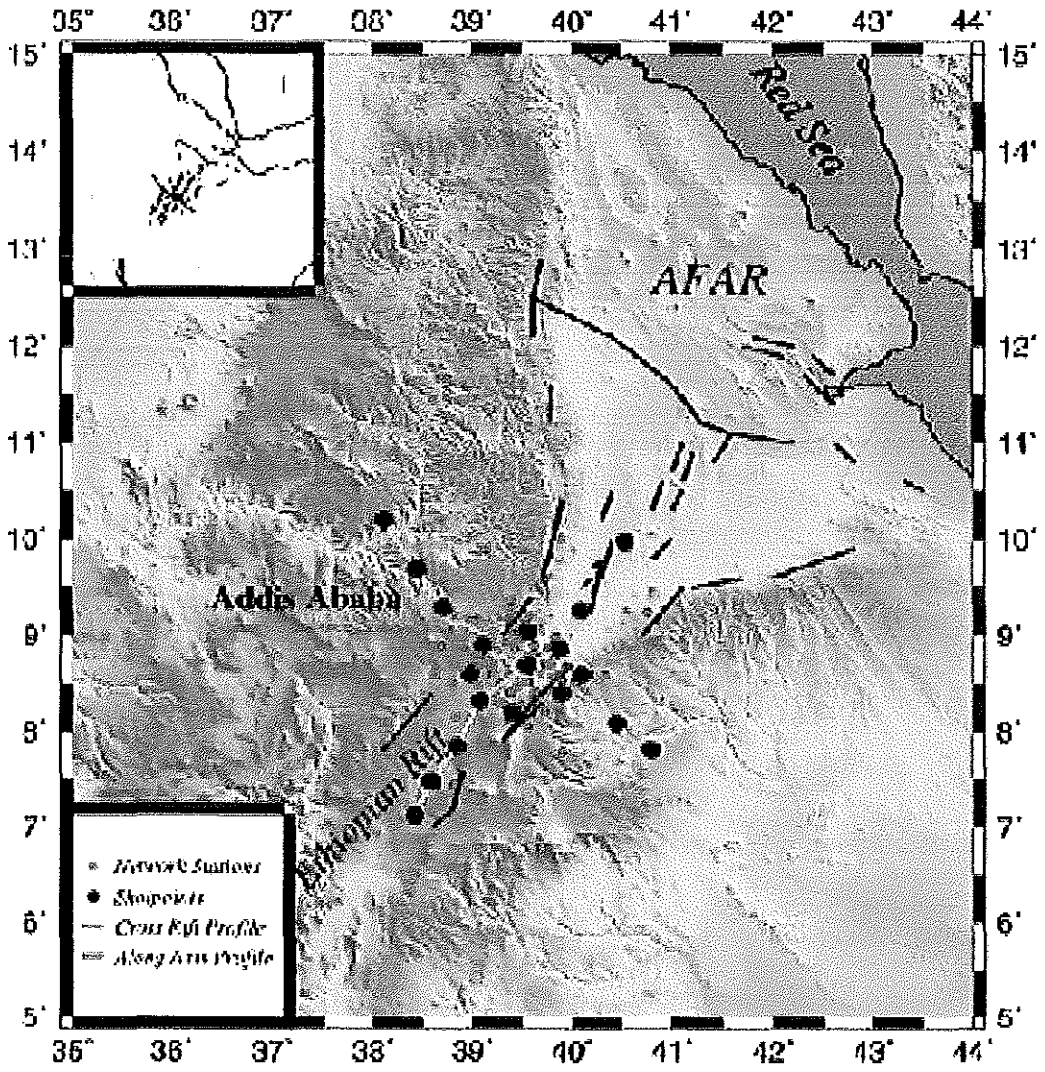

Fig 3.1. Study area-showing profiles 1,2 and 3.

The work was started in 2001 and finished by 2003. It involved recording of seismic "echoes" from the controlled explosions and natural earthquakes, to provide an image of the top 100km or so of the earth over a region encompassing the northeastern part of the main Ethiopian rift were it enters afar. This project was divided into three phases where phase-I involved 30 long term continuously recording seismic instrument being deployed over an approximately 250 x 250km^2 centered on the volcanic segment in the rift valley

phase-I involved 30 long term continuously recording seismic instrument being deployed over an approximately 250 x 250km^2 centered on the volcanic segment in the rift valley immediately to the north-east of the town of Nazareth. Phase-II began in September 2002 and involved the deployment of a further 50 recorders within the phase-I array, concentrating the density of recording the center of this region, in particular to study local earthquakes to refine our understanding of the patterns and origin of the local seismic activity.

3.2. The controlled source phase of the project

Phase-III was the controlled source seismic study and was undertaken in January 2003. This project involved the deployment of nearly 1000 recorders over an 8-day period, which instruments will record the seismic waves generated from the detonation of 19 charges on both boreholes and lakes.

The instrumentation used in the project included two different types of seismic recorders, Guralp 6-TD broadband systems and RefTek Texan recorders.

The Guralp 6-TDs come as a bundle with a 12V dry cell battery, solar panel, to energize these seismometers and a GPS clock receiver to synchronize their time round the clock. They were buried level and oriented north in a hole approximately 50-75cm depth. They were deployed at a nominal spacing of 4 – 5km.

Both the Guralp 6T-Ds and the RefTek Texans were deployed using a deployment sheet. This sheet not only helped in the easy recovering of the seismometers but also to identify the location of each seismometer for the understanding of data it has recorded.

4. BASICS OF THE METHODS USED IN THIS WORK.

4.1. Seismic Waves

Seismic waves are messengers that convoy information about the earth's interior. Basically, these waves test the extent to which earth materials can be stretched or squeezed somewhat as you can squeeze a sponge. They cause the particles of the material to vibrate, which means that these particles temporarily stretched out of position as they move back and forth. The capacity of a material to be temporarily deformed by passing seismic waves can be described by its property of *elasticity*. These physical properties can be used to distinguish different materials. They influence the speed of the seismic waves through those materials.

Seismic sources may be natural (uncontrolled), for example earthquake or artificial (controlled), for example explosives. Controlled source seismology involves the detonation of seismic explosive charges in deep boreholes distributed along a profile of seismic recording instruments deployed at regular intervals along the surface. The seismic waves generated by the charges travel down into the crust of the earth and are reflected and refracted back to the surface from geological interfaces in the earth. The seismic instruments record the resulting seismic wave as they reach the surface of the earth along the profile.

During explosion many seismic waves are generated. These waves are get both refracted and reflected. Of these waves only the refracted p-waves will be treated in this work.

4.2. Basic properties of seismic wave propagation

Depending on their depth of propagation seismic waves are divided as body waves and surface waves. As their name implies, the former one can travel directly through a mass of some substance in any direction, and the latter can travel only near the surface of such a mass, or close to the border between two different substances. Body waves are further subdivided into two namely P and S waves while surface waves are divided into Raleigh and Love waves.

Seismic elastic wave is a form of energy, which travels through a medium depending on its elastic property. It is by vibrating the particles of the medium that seismic waves travel inside the earth. Energy could be released from a controlled source which could be a mere smite of the surface by a hammer or through the detonation of explosives inside a borehole as treated in this work. One the other hand, the energy could also be natural such as earthquakes. The way in which this energy is disseminated is in the form of seismic waves emanating from the source traveling outward in a spherical way.

P (primary)-waves also known as *compressional/ longitudinal* waves; travel by vibrating the particles of the medium in the direction of their propagation. Their names are typical of their behavior for the particles are vibrated in a continuous rarefaction and compression and their first arrival on the seismographs.

S (secondary) - waves are also named as *shear/ transversal* waves; travel by vibrating particles of the medium in the direction that is perpendicular, or transverse, to their direction of propagation. As their name implies S- waves arrive on the receivers after P-waves.

4.2.1. Seismic wave conversions

When a wave reaches a boundary between two substances in which the wave speeds are different it divides into waves that bounces, or *reflect*, from the boundary and other wave that pass, or *refract*, across the boundary. The original wave that travels to the boundary is called the incident wave. At the boundary, it is converted into reflected and refracted P-waves and S-waves that travel away from the boundary in different directions.

Observe, for example, that an incident P-wave converts into both reflected and refracted S-waves as well as P-waves *(Fig. 4.1)*.

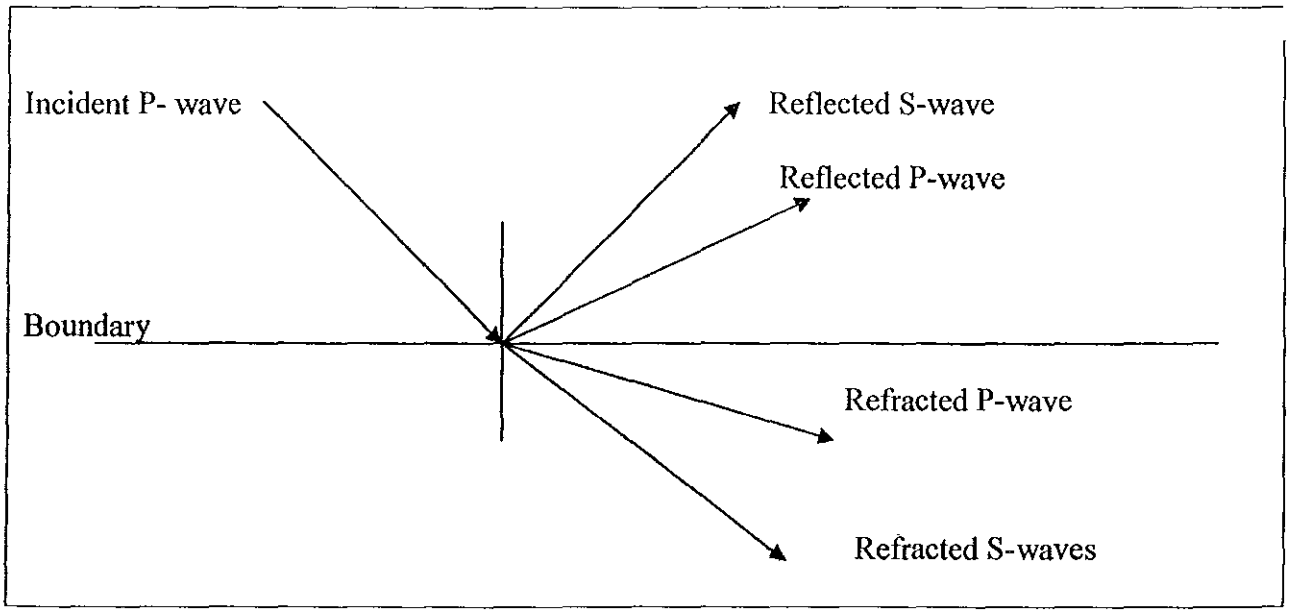

Fig. 4.1. Wave conversions at the boundary.

4.2.2. The law and principles of seismic waves.

While they travel through the earth seismic waves follow the following three natural laws:

4.2.2.1. Snell's Law

Snell's law states, "The directions of the reflected and refracted waves traveling away from a boundary depend on the direction of the incident wave and the speeds of the waves". It governs the direction of all reflected and refracted P- and S-waves produced by an incident P-wave or an incident S-wave.

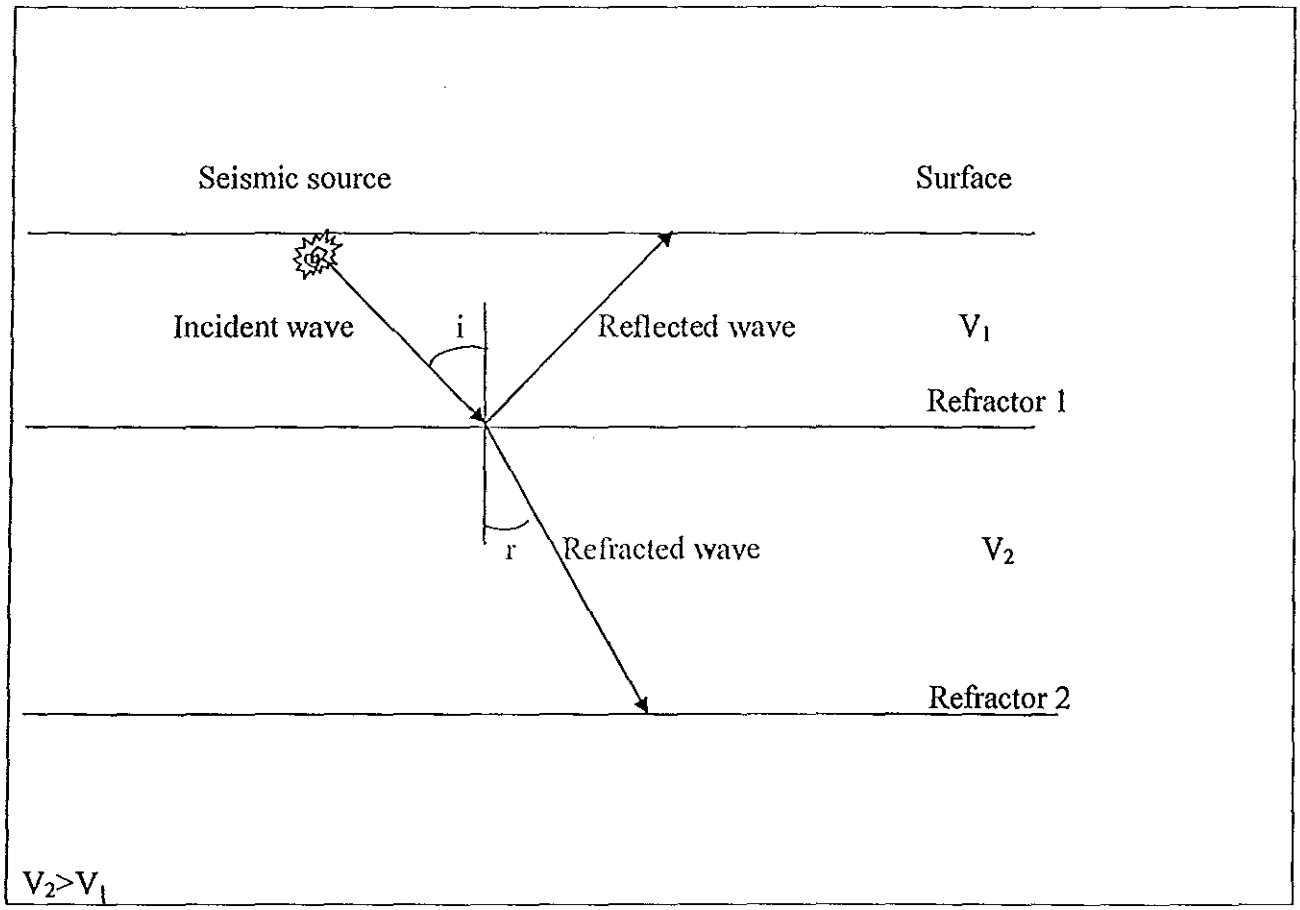

Fig 4.2. Diagram showing how seismic waves refract at an interface

$$\frac{v_1}{v_2} = \frac{\sin i}{\sin r}, \quad \text{.....Eqn 4.1}$$

Where, v_1 is the speed of the wave in the first medium; and

v_2 is the speed of the wave in the second medium.

Equation 4.1 is also known as the *Snell's law.*

The critically refracted wave is produced by an incident wave traveling along the ray that reaches the boundary at the *critical angle of incidence i_c.*

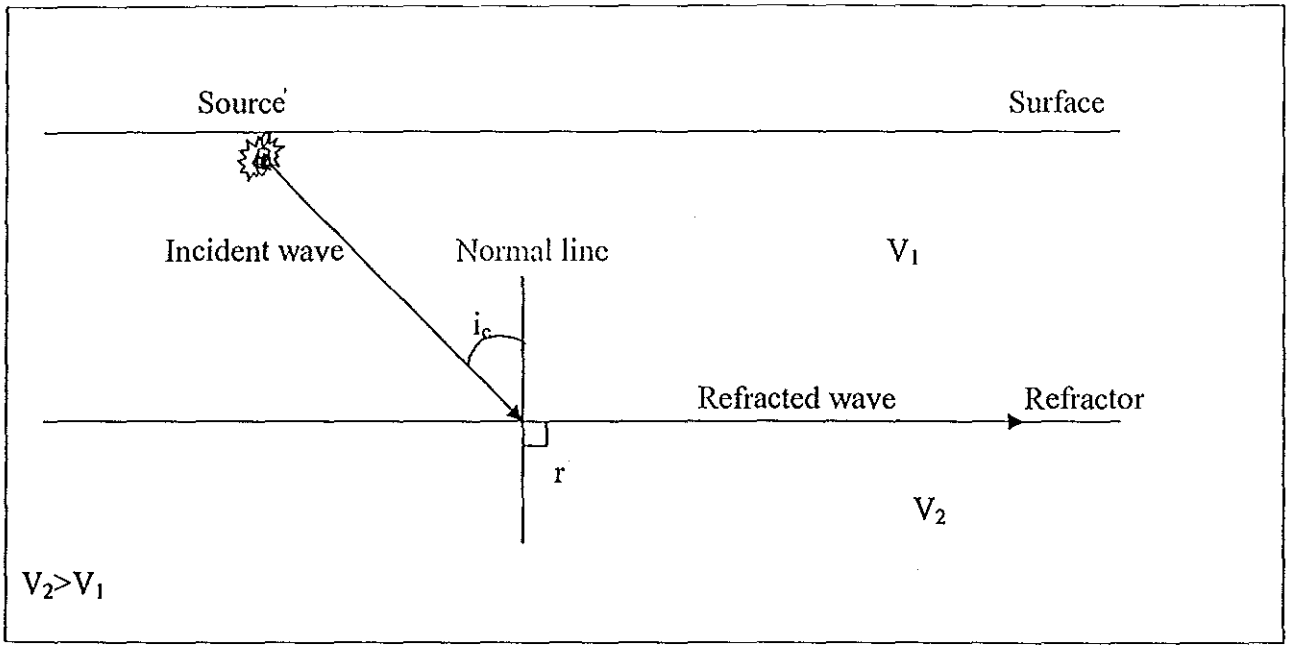

Fig 4.3. A critically refracted wave on horizontal smooth refractor.

Figure 4.3 shows that at critical angle of incidence, the wave is refracted in a horizontal direction or is "critically refracted". For this case of critical refraction, sin r = sin 90° = 1, hence Snell's law becomes:

$$Sin\ i_c = \frac{v_1}{v_2}, \quad \text{.....Eqn 4.2}$$

It is worth noting from equation 4.1 the following three points,

a) If $v_1 = v_2 \rightarrow i = r$, *then there is no refraction.*

b) If $v_1 > v_2 \rightarrow i. > r$, *then there is no way we can record the refracted waves.*

c) If $v_1 < v_2 \rightarrow i < r$, *then the refracted waves go up to the surface.*

4.2.2.2. Huygen's principle

This principle states "every point in the wave front is a source of new waves that travel away from it in all direction". That is critically refracted wave is made of infinite amount of point explosions, which simulate infinite amount of explosions inside the earth. Hence energy from within the earth is again released and reaches the surface to be recorded.

4.2.2.3. Fermat's principle

The principle asserts "elastic waves travel between two points along paths requiring the least time". That is, after the seismic energy has been critically refracted and started to rise up according to Huygen's principle, then again, it is the ray with an angle equal to the critical angle of incidence that reaches the surface first. Mathematically, it is shown below.

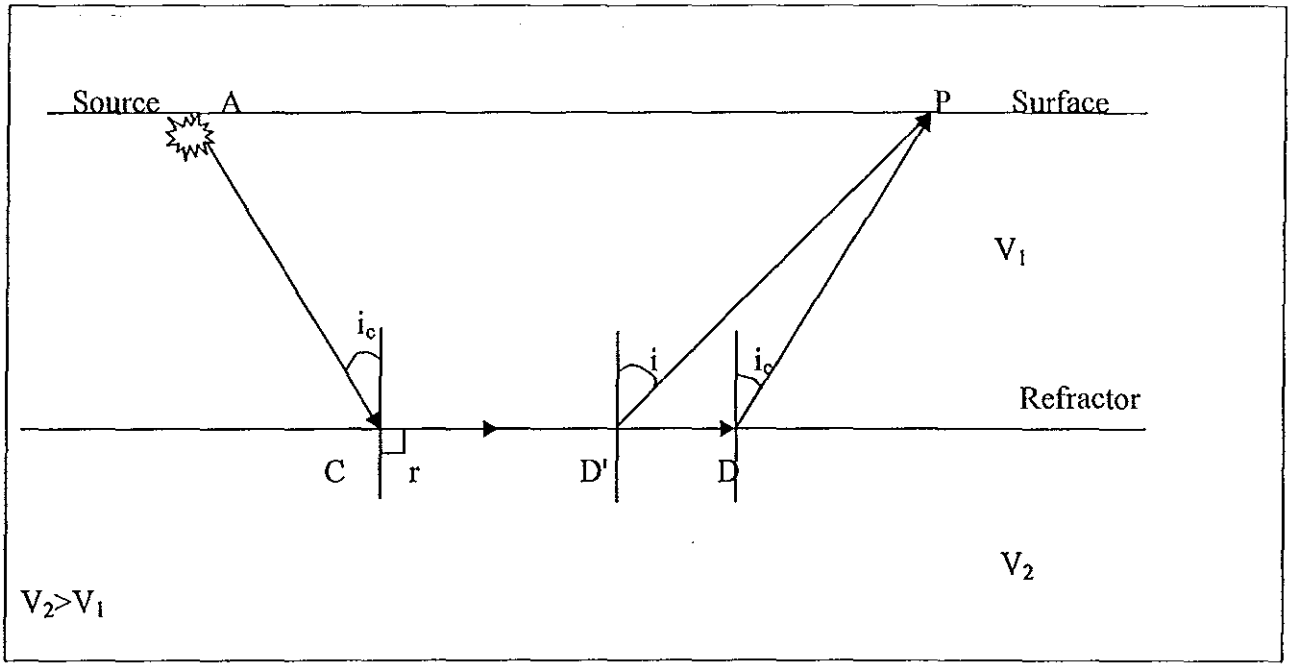

Fig.4.4. Two different waves emerging from the same refractor at different angles of refraction.

Let the time taken for the wave to travel along the path ACDP is t_1 and the time taken for the wave to travel along the path ACD'P is t_2. Mathematically their values can be calculated as follows:

$$t_1 = \frac{AC}{v_1} + \frac{CD}{v_2} + \frac{DP}{v_1}$$

$$t_2 = \frac{AC}{v_1} + \frac{CD'}{v_2} + \frac{D'P}{v_2}$$

$$t_1 - t_2 = \frac{z}{v_1 \cos i'}\left[\cos(i_c - i) - 1\right], \quad \text{.....Eqn 4.3}$$

As $t_1 < t_2$ the path followed by the wave, according to Fermat's principle will be Path I. And hence the seismic wave that arrives first is the refracted wave, which has the same angle as the critical angle of incidence.

4.3. Generalized Reciprocal Method (GRM)

The Generalized Reciprocal Method (Palmer, 1980) is an inversion technique, which uses travel-time data from both forwarded and reverse shots and which provides a graphical solution to resolve the geometry of sub-surface refractors. The method uses refraction migration to obtain the detailed structure of the refractor and information about any localized lateral variations within it. Refraction migration uses the offset (migration) distance, which is the horizontal separation between a point on the refractor where a ray is critically refracted and that at the surface where the ray emerges.

It has been pointed out (Sjogren, 1984), however, that the migration distance does not satisfactorily define narrow zones with low seismic velocities. As such zones are often the targets for refraction surveys, it is important that the interpretational method is capable of resolving them. Palmer, (1999) has demonstrated that the migration distance selected to define the refractor surface is not necessarily the same as that which provides the optimum information about the refractor velocities. Consequently, if the GRM is used to its full effect, it can be used successfully to define narrow low velocity zones. In order to increase the accuracy of the GRM, Zanzi (1990) has proposed that consideration should be given to nonlinear corrections in the case of an irregular refractor.

A principal difference of the GRM compared with the plus-minus method is that the critically refracted rays emerge at or very near the same point on the refractor, thereby removing the smoothing problem. They arrive at two different geophone locations separated by a distance XY *(Fig. 4.5)*.

Two functions are computed within the generalized reciprocal method: the velocity analysis function (t_v) and the time depth function (t_G). The latter is determined with respect to a position G (Fig. 4.5) at the midpoint between the points of emergence at the surface of forward and reverse rays at Y and X, respectively. Both functions are expressed in units of time and are detailed below. In cases where the maximum angle of dip is the less than 20^o, the GRM, as detailed here, provides estimates of refractor velocities to within 5%.

Gremix is a software package designed to assist in the interpretation of seismic refraction data in terms of a laterally varying earth structure. It combines the features of the Plus-Minus method of Hagedoorn (1959) with the features of the Generalized Reciprocal Method (Palmer, 1980) to provide a user friendly means of entering, editing, interpreting, and producing annotated hard copy results of seismic refraction first arrival data.

The Generalized Reciprocal Method uses arrival times from opposite shots (one forward and one reverse) which travel along the same refractor, along with the reciprocal time between the shots, to determine the time depth from a surface geophone to the refractor.

This method was first developed and later introduced by the Australian scientist Derecke Palmer at the 50^{th} annual international SEG meeting in November 18, 1980, Houston. The GRM is a technique for delineating undulating refractors at any depth from inline seismic refraction data consisting of forward and reverse travel times.

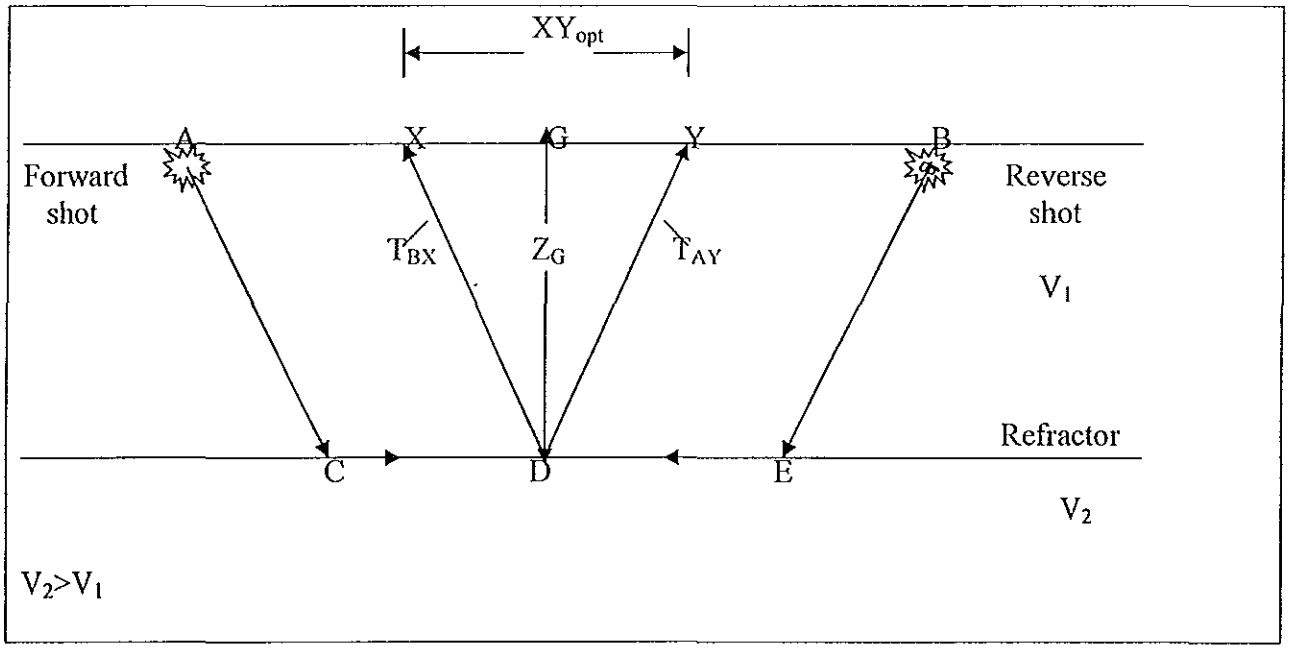

Fig 4.5. Diagram showing parameters used in GRM

The travel times at two geophones, separated by a variable distance XY *(Fig 4.4)*, are used in refractor velocity analysis and time depth calculations. At the optimum XY spacing, the upward traveling segments of the ray to each geophone emerge from near the same point on the refractor. This results in the refractor velocity analysis function being the simples and the time-depth being the most detail.

The GRM provides a means of recognizing and accommodating undetected layers provided an optimum XY value can be recovered from the travel-time data, the refractor velocity analysis, and or the time depth. The presence of undetected layers can be inferred when the observed optimum XY value differs from the XY value calculated from the computed depth section. Using an average velocity based on the optimum XY value can accommodate the undetected layers. This average velocity permits accurate depth calculation with commonly encountered velocity contrasts *(D. Palmer 1980).*

4.3.1. Optimum XY value

Both the velocity analysis and time-depth functions are evaluated and presented for a range of XY values from zero to one considerably larger than the optimum value. The increment in values of XY is usually taken as being equivalent to the geophone separation. Thus, if the geophones are spaced at 5 m intervals, XY is incremented in steps of 5 m.

At the optimum value of XY, both the forward and reverse rays are assumed to have been critically refracted at or very near the same point on the refractor. The optimum XY in the analysis of velocity is determined as being that which gives a time-depth function which approximates most closely to a straight line. Where there are lateral variations in refractor velocity, the optimum velocity value of XY may differ with distance. In the selection of the optimum value of XY for the time-depth function, the graph that exhibits most detailed should be the one chosen. In general, the optimum value of XY should be the same for both the velocity analysis and the time-depth functions

The optimum XY value is obtained based on the velocity analysis function t_v *(Eqn 4.4)* being the smoothest and the time depth function *(Eqn 4.5)* being the most detailed.

$$t_v = \frac{t_{AY} - t_{BX} + t_{AB}}{2} \quad \text{..... Eqn 4.4}$$

Where; t_v *is velocity analysis function*

t_{AY} *is forward time from shot A to the geophone at Y*

t_{BX} *is Reverse time from shot B to the geophone at X*

The shot geophone positions are shown in figure 4.4. The plot of the velocity analysis curve verses offset would be smooth because at the optimum XY value, the seismic wave refracts from nearly the same point.

$$t_G = \frac{1}{2}\left[t_{AY} + t_{BX} - \left(t_{AB} + \frac{XY}{v'_n}\right)\right], \quad \text{Eqn 4.5}$$

Where; t_G is time depth function.

v'_n is apparent velocity determined from the velocity function.

By time depth function, it can be defined as the measure of measure of depth to the refractor in units of time. This function is converted as depth in units of space using equation 4.6

$$t_G = \sum_{j=1}^{n-1} Z_{jG} \frac{(v_n'^2 - v_j'^2)^{\frac{1}{2}}}{v'_n v'_j}, \quad \text{Eqn4.6}$$

Where Z_j gives us the layer number. Note that t_G is measure of depth in units of time and Z_G is measure of depth in units of space. Hence,

$$Z_G = t_G\, DCF$$

Where, DCF is depth conversion factor.

The optimum XY value we obtained using the above two functions is known as the observed XY value. XY value is then calculated using the apparent velocity obtained the velocity function using the equation 4.7

$$XY_{opt} = 2\sum_{j=1}^{n-1} Z_{jG} \tan \theta_{jn,} \quad \text{.....Eqn 4.7}$$

$$\text{Where, } \theta_{jn} = \sin^{-1}\left(\frac{v_j}{v_n}\right)$$

The XY value we observe and calculate should be the same to an acceptable limit. If not then it implies that there is a hidden layer present.

- *If* $XY_{calc} = XY_{obs}$ *(No hidden layer)*
- *If* $XY_{calc} > XY_{obs}$ *(Velocity inversion)*
- *If* $XY_{calc} < XY_{obs}$ *(Thin layer)*

Hence once a hidden layer is observed, then the average velocity is used to map the hidden layer. This average velocity is defined in equation 4.8 below;

$$\bar{v} = \left[\frac{v'^2_n XY_{opt}}{XY_{opt} + 2t_G v'_n}\right]^{\frac{1}{2}}, \quad \text{.....Eqn. 4.8}$$

Where, $\bar{v}$ *is average velocity.*

and depth to the refractor is defined in Equation 4.9,

$$Z_{ref} = \frac{t_{G\bar{v}}}{\cos\theta}, \quad \text{.....Eqn 4.9}$$

Where, Z_{ref} *is depth to the refractor, and* $\theta = \sin\left(\frac{\bar{v}}{v'}\right)$

5. DATA ACQUISITION

5.1. Drilling of boreholes

The Ethiopian drilling company, Saba Engineering Plc. was given the contract to drill six scientific wells in July 2002. The holes were drilled to be 10" in diameter and 50 m deep, though this configuration was not kept at some drill sites. The drilling was conducted by the use of rotary rigs where all the wells were drilled through the use of DTH (*Robinson, 1992*) methods. At sites where more than one hole was drilled, the distance was kept at a minimum of 45m so that the explosion from one would not detonate the charge in the other hole. Two holes were drilled at sites where they were needed to produce a higher energy from the detonation. Drilling of the wells was finished by January 2003.

The holes drilled were far away from tukuls, cottages, buildings, bridges, underground pipelines, electric mains, etc. This was to ensure the safety of the communities and there infra structure. The location of the shot holes after optimizing safety and higher s/n ratio is shown in Table 5.1.

Shot point	Site name	Easting	Northing	Zone	Elevation
24	Koka	500547	920584	37P	1602
25	Doni B	568063	843141	37P	1236
26	Beseka	594590	976028	37P	953
27	Melka Sedi	269036	483788	37P	898
28	Gewane	679730	1129583	37P	555

Table 5.1 Shot points with their position and elevation.

5.2. Deployment and shooting phase

5.2.1 Seismic sources

Sources of seismic energy come in a variety of sizes and shapes. Anything that causes motion on the ground could be defined as source of seismic energy. The type of seismic energy source used for this source was considered and is described below.

Advantages: -

- These types of sources impound the highest amount of seismic energy, which are a direct unction of the type and size of the explosives used.
- The energy tends to be of very high frequency.
- These types of sources are usually placed inside a borehole, which tends to reduce the generation of surface waves.
- Explosive sources are repeatable.

Disadvantages: -

- Safety
- Obtaining permission to using these sources is difficult.
- Data acquisition using this sources is much slower than using other sources.
- This is primarily because boreholes must be drilled within which explosives are t be placed.
- Explosives tend to be expensive to acquire and maintain.

5.2.2 Shot details

The whole procedure of transporting the explosives, unloading them at their respective sites, shooting them and returning to Addis Ababa lasted from January 9 to the 15th 2003. The shots were conducted between January 11 and 13 *(Table 5.3)*. The explosives and their accessories that were transported to the site include;

1. 8.4-ton powergel c+ *(Fig 5.1(a))*, where the main explosive is packed in 25kg boxes each is containing two12.5kg packages of diameter 210mm and length 300mm.
2. Multi prime boosters, each 0.5kg to detonate the power gel.
3. Cordtex *(Fig 5.1. (b))* detonating or primcord, to connect the boosters.
4. Electric seismic detonators *(Fig 5.1. (c))* to initiate the explosives.

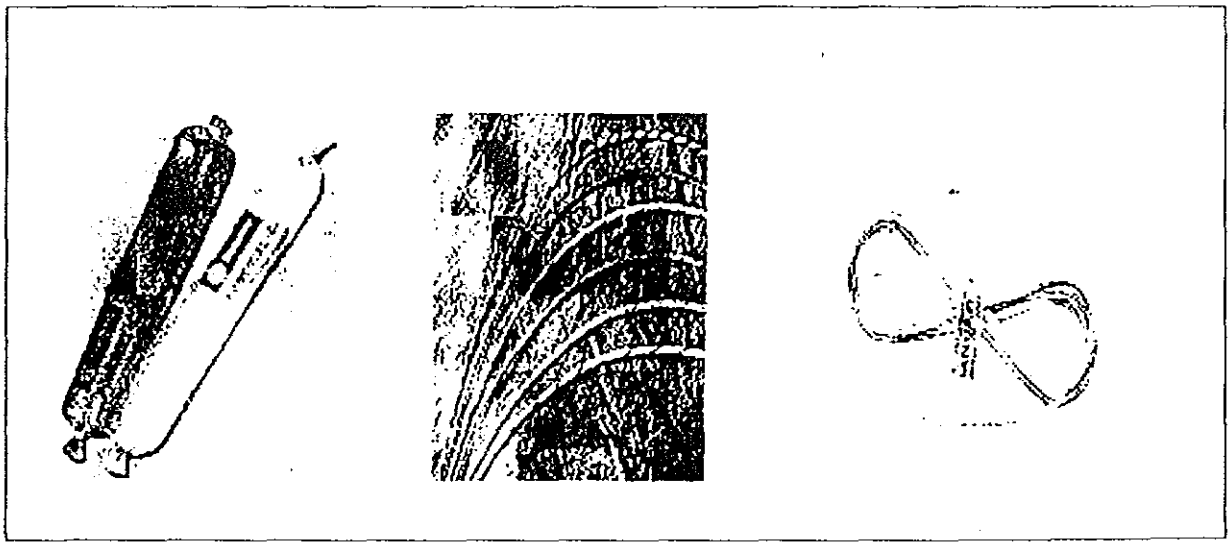

(a) (b) (c)

Fig.5.1. (a) Power gel C+, (b) Cordtex Wires, (c) Seismic detonators

The power gel C+ (*Fig5.1 (a)*) explosives were buried to 30m of the surface (*Table5.2*). The boosters were positioned at regular intervals along the length of the hole. The primacords were connected along the whole length of the hole where their ends were tightly tapped together to the detonator.

The top part of the hole was stemmed according to the EAGLE specification. The specification was two part of 15mm angular chippings to one part of wet sand to provide containment and to prevent blowout. The holes were stemmed with 3 Cu m of stemming. The stemming was needed in part to: -

1. Contain the explosion into the ground so that there would not be any damages caused to humans or property

2. If the explosion is contained in the ground, it also gives higher energy, which is directly related to more energetic shock waves.

Shot point	Location	Target Gel to be loaded	Actual Gel weight loaded	Notes
24	Koka	1000	525	Short-loaded due to safety reasons.
25	Doni B	1500	1025	Short-loaded due to safety reasons.
26	Beseka	1000	1150	Almost normal-loaded since it is safe.
27	Melke Sedi	2000	1850	Short-loaded because of partial blockage of hole either before or during loading.
28	Gewane	1000	1000	Normal-loaded since it is safe.

Table 5.2 Shot points with amount of charge loaded.

The time of blast for each shot *(Table 5.3)* was precisely set on the shooting boxes, which had satellite *(EL-Paso or USGS)* timers they are synchronized with the recording Texans. All the charges were detonated after 12.00 mid night local time, times where signal noise ratio (S/N) was considered to be high.

Shot point	Site name	Shot date	Shot time (GMT)	Timer
24	Koka	13-Jan-03	21:50:00	El Paso
25	Doni B	12-Jan-03	21:50:00	El Paso
26	Beseka	14-Jan-03	21:40:00	USGS
27	Melkẽ Sedi	12-Jan-03	21:40:00	USGS
28	Gewane	11-Jan-03	21:40:00	USGS

Table 5.3. Shot points; shot time, shot date and timer.

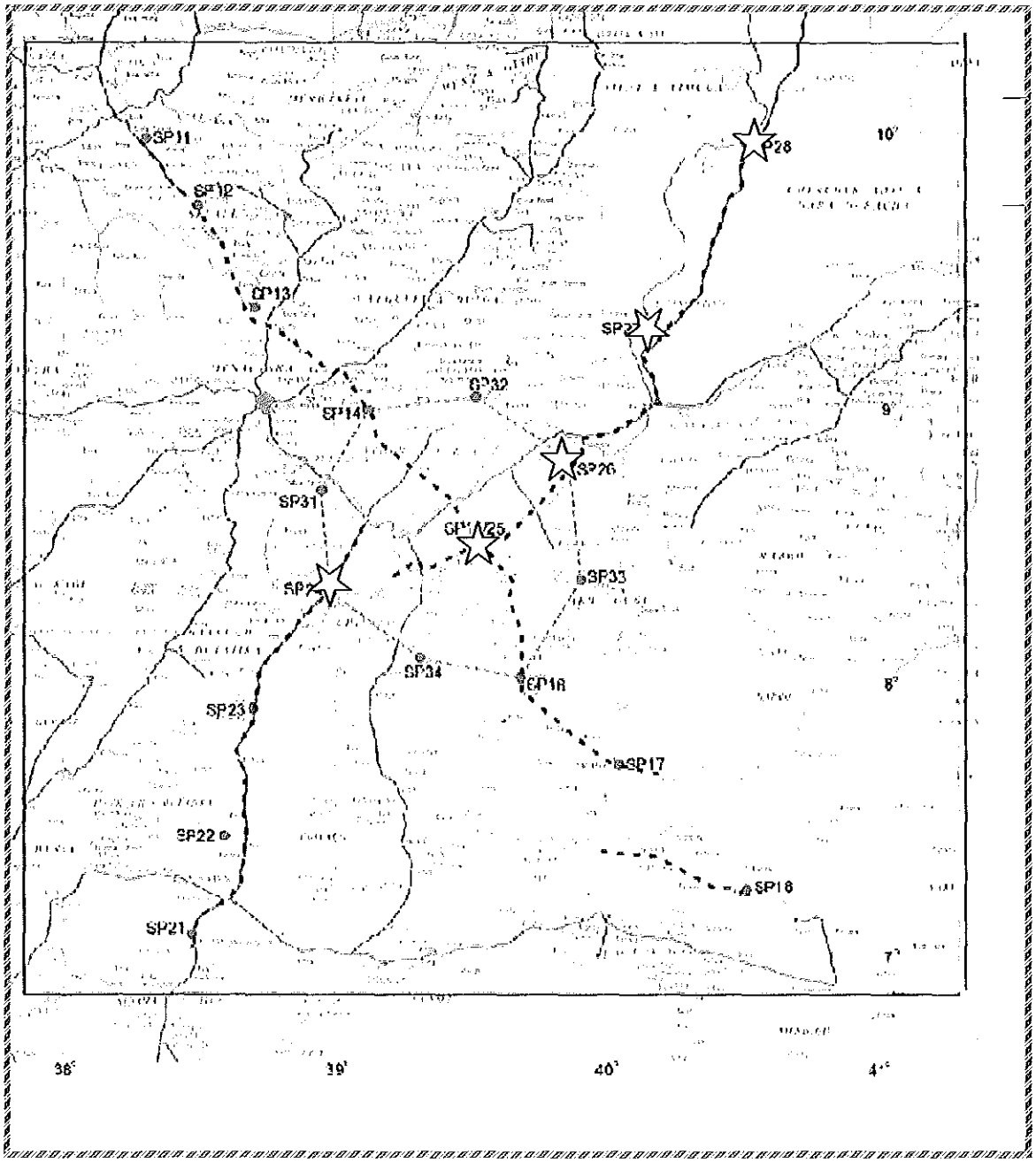

☆ Indicates shots points

Fig. 5.2. Location map of the study area

Generally the altitude of the study area decreases when we go from the southern most of the MER to northern most of Afar *(Fig 5.3).*

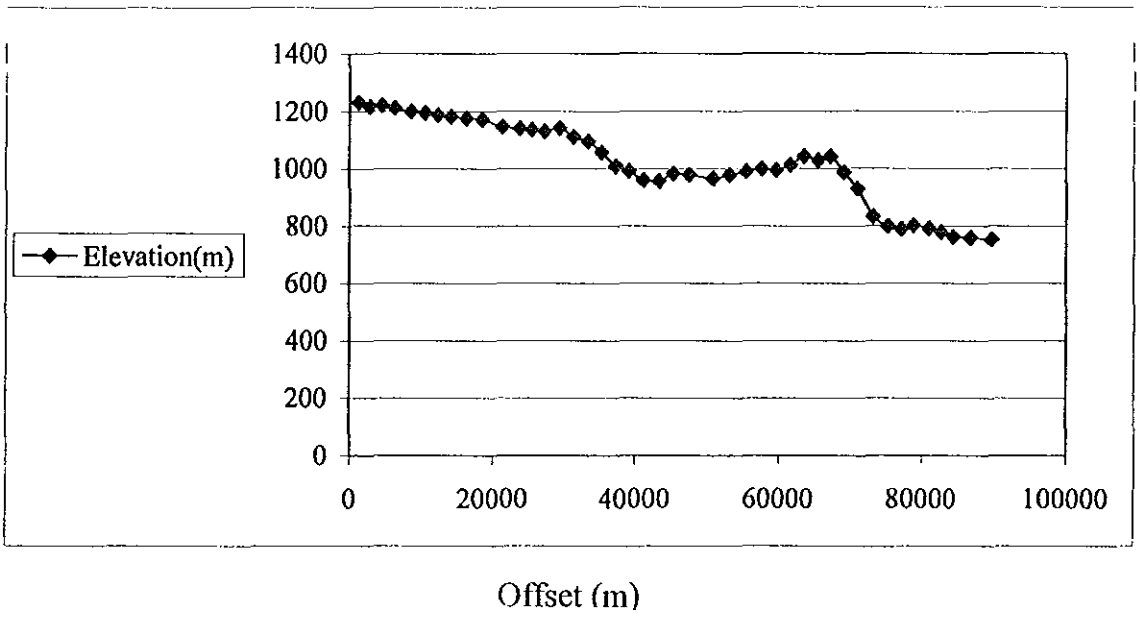

Fig 5.3. Diagram showing the section of the study area.

5.2.3 Ref Tek 125-01 "Texan"

The name Texan *(Fig 5.4)* is given to a miniature seismic recorder, which is produced from a Joint project among the Texas Universities seismic instrumentation alliance *(which includes the Universities of Texas at EI Paso, Rice University and the University of Texas at Dallas).* The Texan is the present day leading edge technology seismic wave recorder

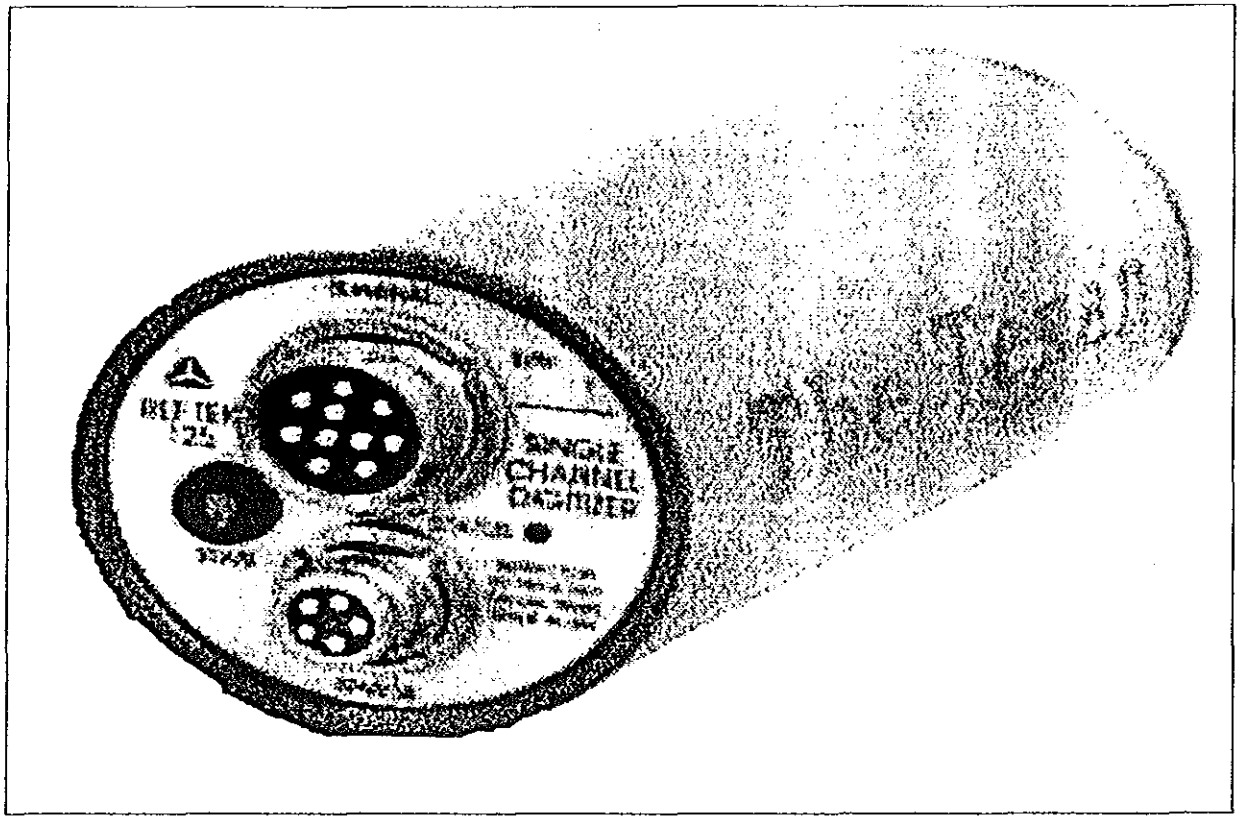

Fig. 5.4. RefTek Texan.

The particular model used in this project is the Ref-Tec 125-01 "Texan". These instruments have been supplied by the University of Copenhagen and IRIS/PASSCAL - University of Texas at El Paso.

5.2.3.1. Features of the Texan

These instruments could be used for:

1. *Active source crustal studies refraction*

2. *Active source crustal studies refraction*

Their features are described briefly below:

1. *Powered from two 'D' cell batteries.*
2. *GPS synchronization.*
3. *Recordings are made based on pre set time windows at a rate of 100 samples per second (SPS).*
4. *Timing accuracies for the recording period must be within +/-5 msec relative to the shot time.*
5. *32 MB data storage capacity expandable to 64 MB.*

5.2.3.2. Instrument operation

Texans feature a low noise differential input amplifier, 24-bit analogue to digital converter. The transit case has many functions in addition to containing storing and transporting the geophones. This transit case includes interconnection cables *(125 bus),* which helps to easily connect to the external control device also known as the Bridge.

Functions of the bridge include:

1. *Transmit data between the 125 bus and the TCP/IP Ethernet bus, which enables the user interface program (UIP) to run on either a windows or Unix work station.*
2. *Routes the 111A GPS receiver/clock signals to each Texan for synchronizing internal time to UTC.*
3. *Supplies power to the Texans for setup and data retrieval.*

After setup, the Texans are deployed for recording. A state LED displays the operation condition of the Texan. Green light indicating that:

1. *Battery voltage is sufficient*
2. *Acquisition program loaded*
3. *The unit is either ready to acquire data or is doing so.*

Red light signifying that one or the whole above functions is not set

5.2.1. Recording instruments deployment phase.

Since the operation of these Texans is dependent on the alkaline batteries, they were programmed to operate to the maximum time available. They were programmed for a one-hour window for each shot and then to stop. The way they were programmed to start recording within the window where when the shots were fired. All the Texans had the same information on when to start and to stop. Their internal clock was synchronized to clock that generates timing pulses using GPS signals.

At an instant attaching them together through the bridge could program any amount of Texans and when the programming is done, they are made to switch to their internal batteries and ready to be deployed. They are designed to be a single channel recorder with a 4.5 Hz geophone attached to them. Their battery life is lasted for eight days where they were deployed for two days, recorded for four days and finally recovered within two days before their battery life is dead.

The deployment was done between January 10 & 11, in the year 2003. When deploying these Texans, the following package went as a bundle:

- *Road Logs – containing directions, distances, and contact details for each site.*
- *Maps – 1:250km and 1:50km maps with sites and routes marked.*
- *Relevant Permission Letters for the deployment region.*
- *GPS with deployment sites way marked where needed.*
- *Instrument Deployment and Recovery sheets.*
- *Letter explaining the project in Amharic, Oromifa, and English to buried with the Texan handed to any locals.*

During deployment, it was done in a manner that they could be easily recovered and yet the site should be one with minimum noise and maximum security. Almost all of the Texans were deployed along side the off road. This was deemed appropriate for easy retrieval.

They were buried in approximately 0.15m depths with the geophone being inserted into the ground with a maximum vertical alignment *(Fig 5.5)*.

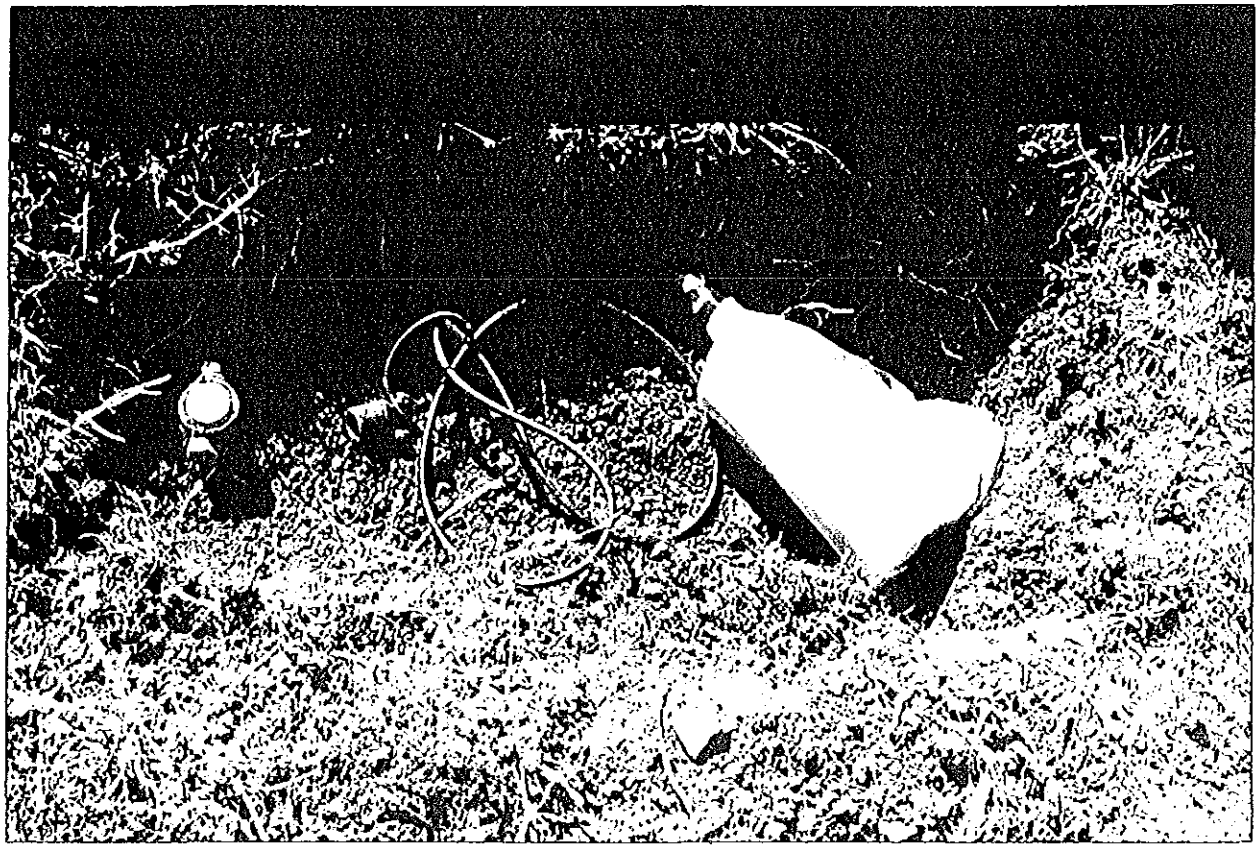

Fig. 5.5. Texan buried inside the ground.

Easting, Northing and elevation data was taken for each geophone *(Appendix 1)*. In addition to this, the station number, the unit serial number, comments, which help the easy retrieval of these instruments, were noted on a sheet. These Texans were deployed in an approximate distance of one kilometer and deployment jumped at the sites where the Gurlap 6–TD *(Sec. 3.2)* seismometers were present.

At the end of the experiment, the Texans are returned to the set up facility, retrieved and the data downloaded to the workstation for processing. The early retrieval phase of these instruments was of crucial importance. This is because; their battery had lifetime of eight

days. After being synched to a GPS clock, these Texans keep track of time using their internal batteries. Though the data is registered with time, it is not the actual time that is registered rather relative.

After being received, the Texans are switched to an external power and the raw SEG – Y data is backed up and later up loaded to a server. When being switched to the external batteries, it is important that the internal batteries are running. If not then there would not be the stop information and the data from the last shot would be useless for that particular Texan.

6. DATA PROCESSING

The data processing includes:

1. *Picking of the first arrivals.*
2. *Converting these first arrival values from their reduced arrival time to their actual arrival time.*
3. *Feeding the arrival times, to the inverting software including information on offset distance and elevation.*
4. *Assigning layers on the travel curves.*
5. *Inversion of the assigned layers to produce the Geoseismic model.*

6.1. Reduced arrival times

Assuming average crustal velocity of 6000 m/s reduced the raw data. The distance of each geophone from the shot was known; hence the traces were reduced in time with the following basic formula.

$$t = \frac{X}{V_c} \quad \text{.....Eqn 6.1}$$

Where, X is offset (distance of the geophone to the shot).

V_c is average crustal velocity i.e. 6000 m/s.

This reduction was imperative because the scale of the experiment was very huge and the attempt to view all the seismic traces would be ludicrous for reasons of scale. Figure 6.1 to 6.5 show reduced arrival times for each geophone from each shot. The picked reduced first arrival time of each geophone lie within the window of –1 to 2 sec *(Fig. 6.1 – 6.5, Appendix 5).*

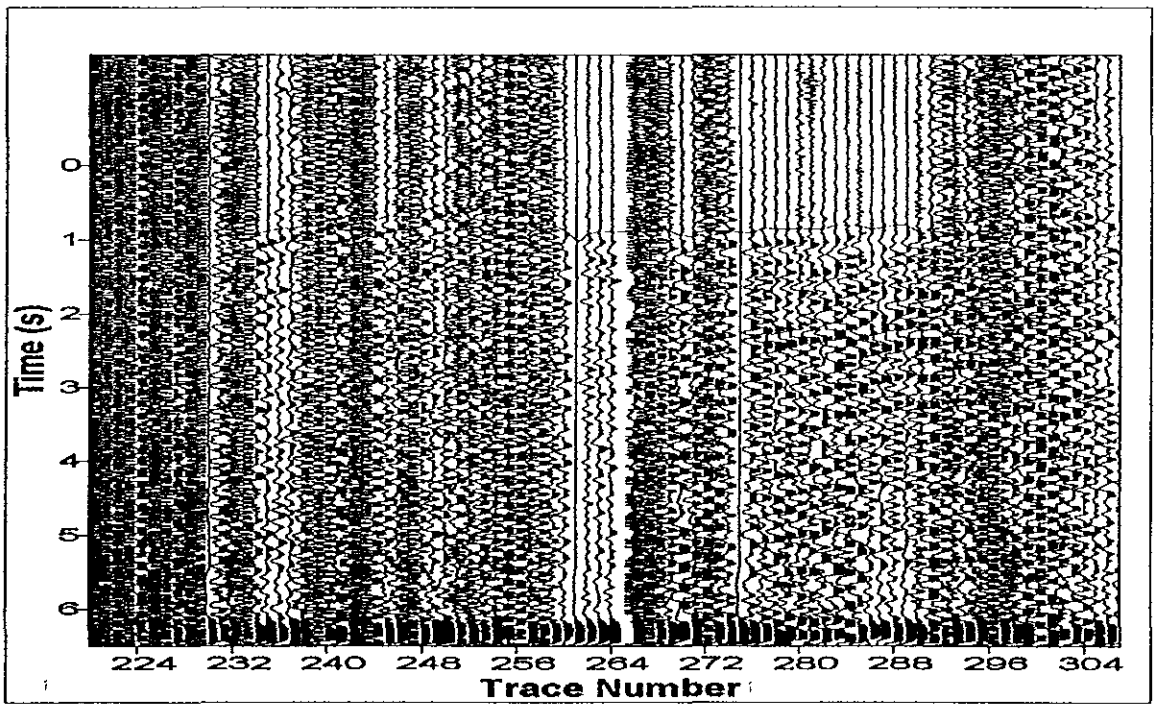

Fig. 6.1. Traces from shot 24.

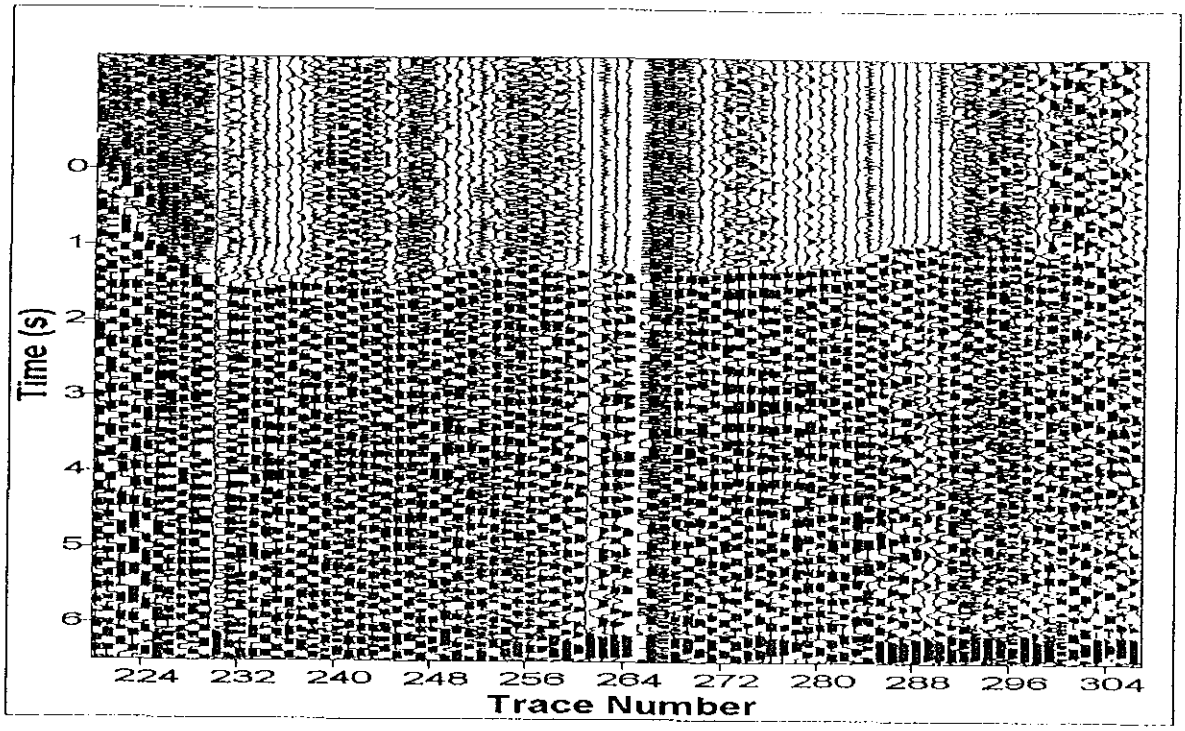

Fig. 6.2. Traces from shot 25.

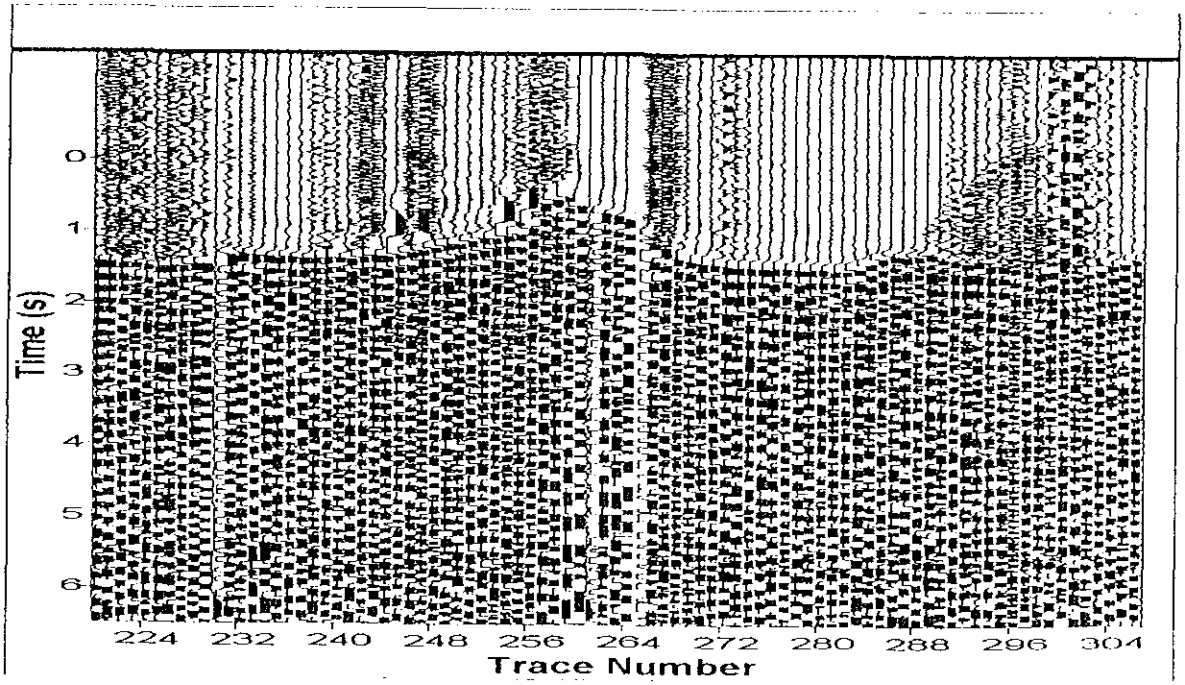

Fig. 6.3. Traces from shot 26.

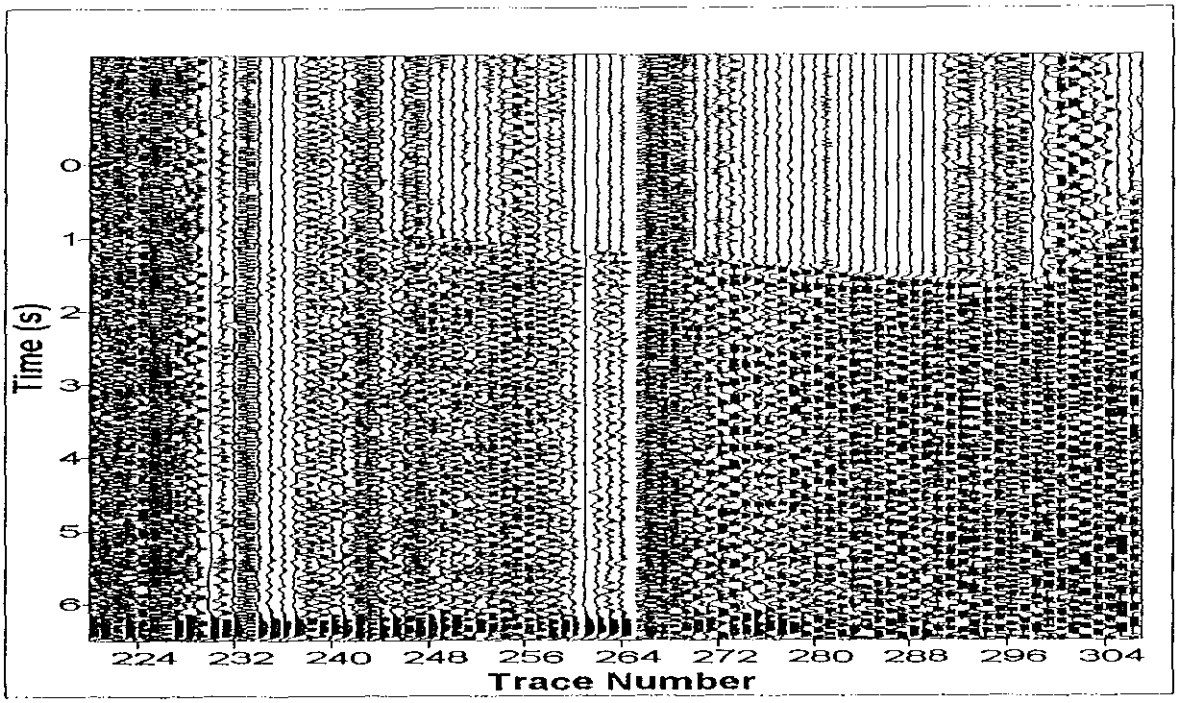

Fig. 6.4. Traces from shot 27.

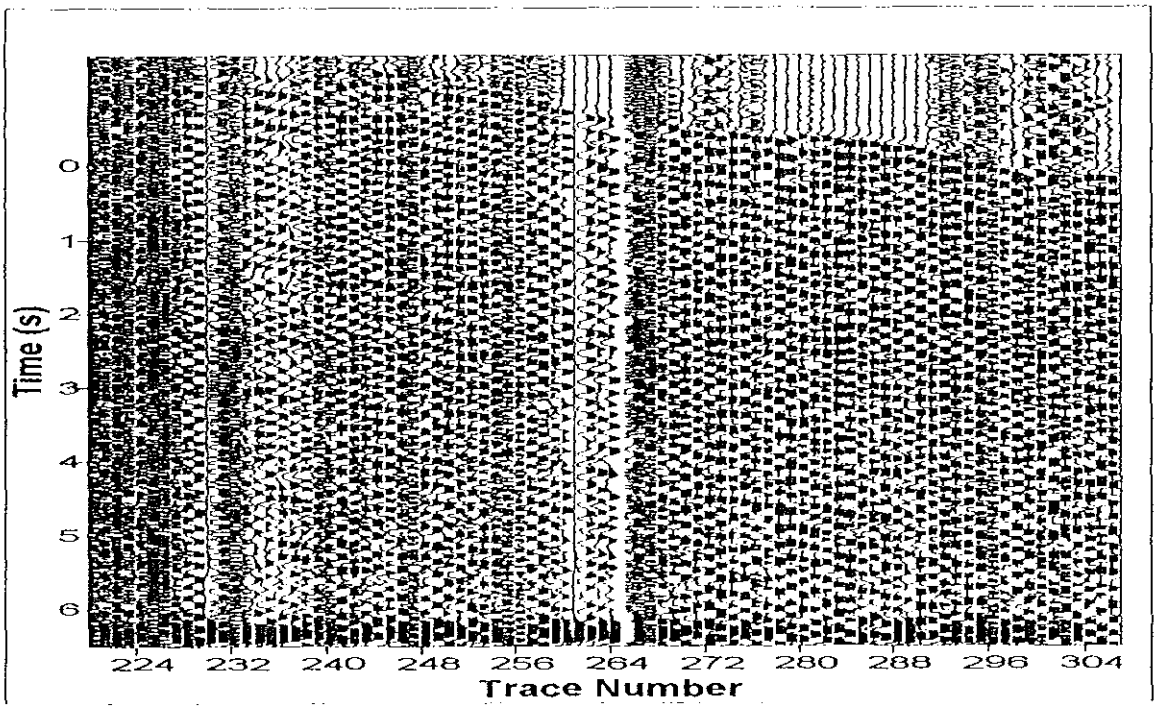

Fig. 6.5. Traces from shot 28.

6.2. Picking of first arrivals

The first arrivals are the refracted crustal p-waves. They were picked iteratively to increase precession. Figures 6.6 & 6.7 show recorded signals with varying degree of signal to noise ratio (S/N).

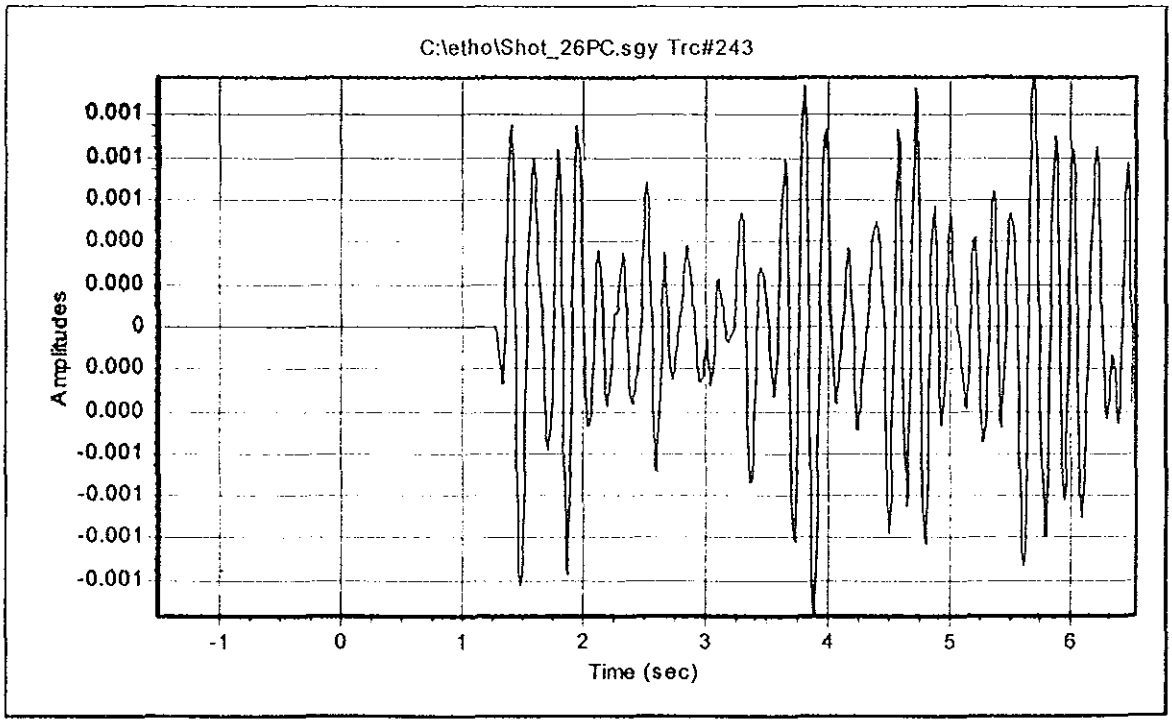

Fig. 6.6. Trace #243 of shot 26, with high S/N ratio.

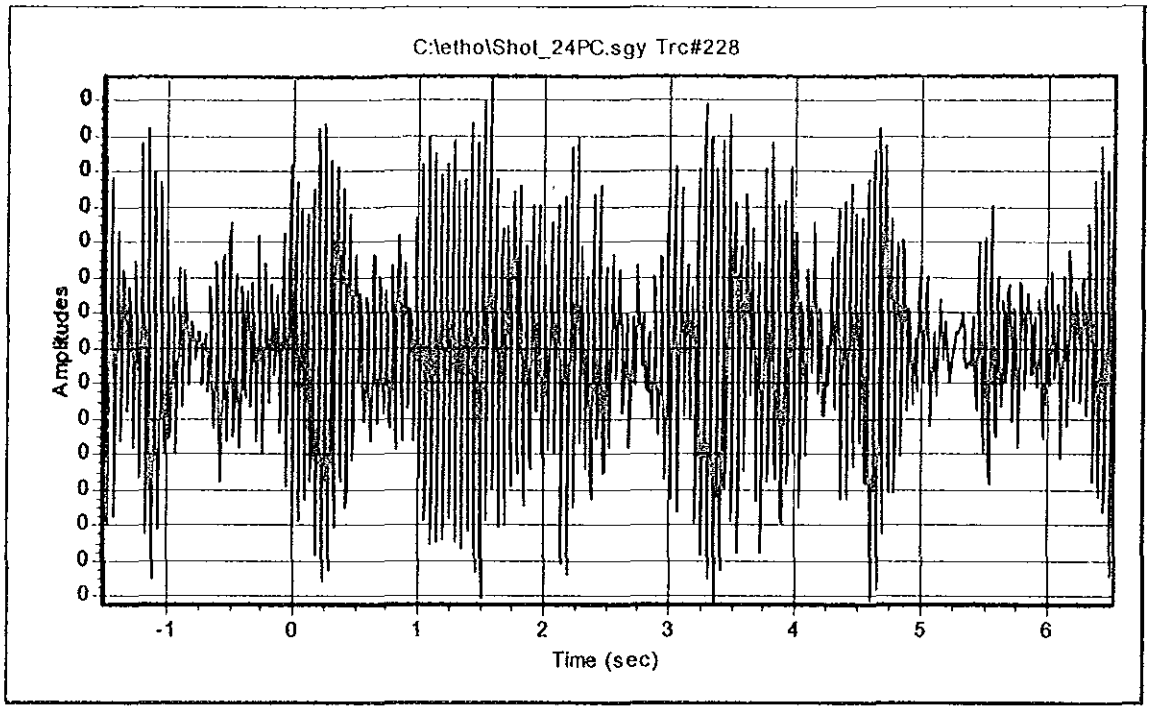

Fig. 6.7. Trace #228 of shot 24, with low S/N ratio.

6.2.1. Raw traces

With the understanding that first arrival time increases with offset, some of the seismic arrivals *(Fig 6.1 to 6.5)* do not follow this principle. The scientific rational is mostly controlled by the difference in altitude between adjacent geophones.

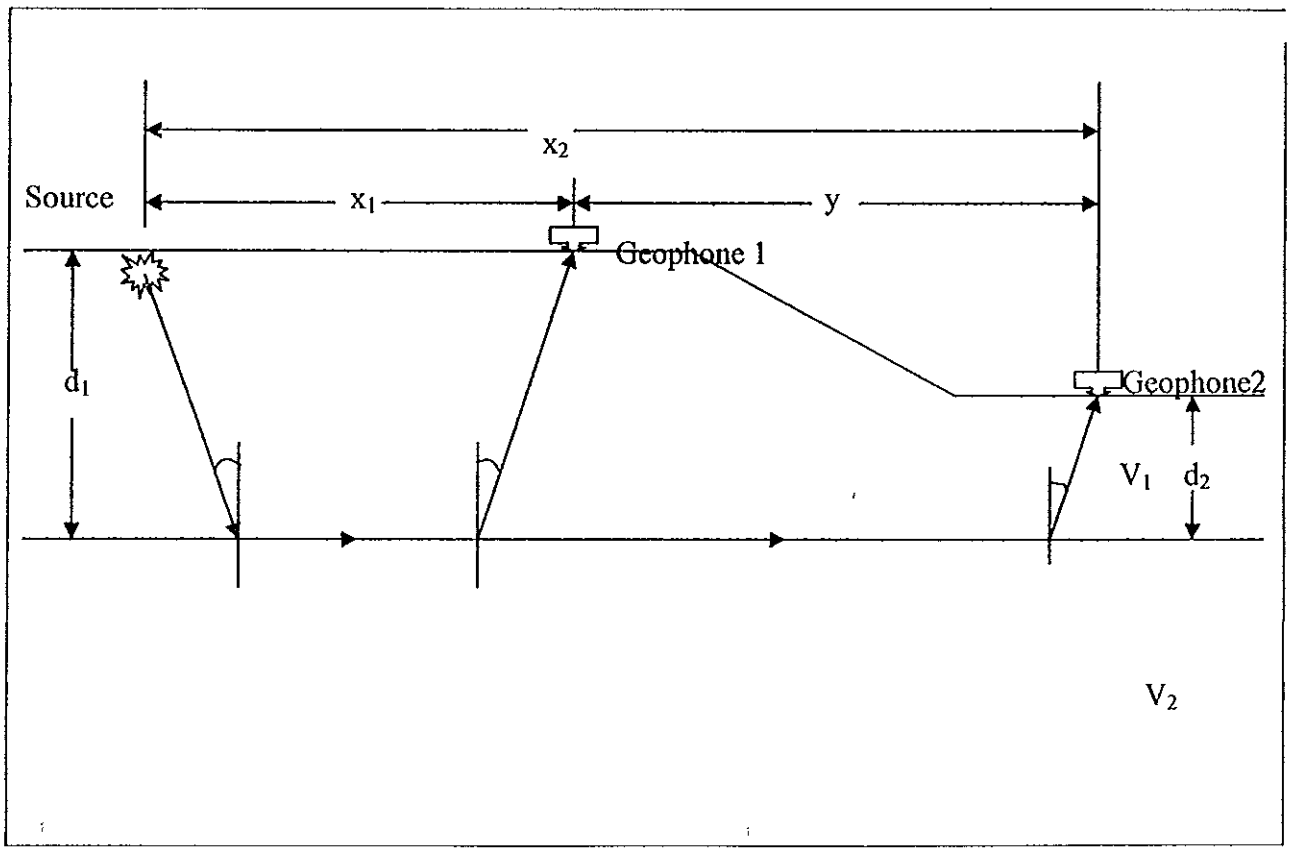

Fig. 6.8 Geophones placed at different elevation.

Though difference in altitude which is also known as statics, controls the arrival times at each geophone, other factors include offset distance between geophone pairs and the velocity contrast between the layers *(Eqn. 6.2)*.

$$\Delta t = \frac{1}{v_1}\left[(d_2 - d_1)\cos\theta + \Delta x \sin\theta\right] \text{----------} \textit{Eqn. 6.2}$$

Where; θ *is critical angle of incidence;*

d_1 *and* d_2, *are depths of the refractor beneath geophone 1 & 2 respectively;*

x_1, *is offset of geophone 1;*

x_2, *is offset of geophone 2;*

Δx, *is difference in offsets of geophone 1 & 2;*

v_1, *and* v_2 *are seismic velocities of the respective layers;*

t_1, *is seismic wave arrival time of the first geophone;*

t_2, *is seismic wave arrival time of the second geophone; and*

Δt, *is the difference in arrival times of geophone 1& 2.*

The difference in first arrival times of the adjacent geophones is less than zero if and only if the following conditions are fulfilled:

$$(d_2 - d_1) < 0; \text{ and } (d_2 - d_1)\,\mathrm{Cos}\theta > \Delta x\,\mathrm{Sin}\theta.$$

Picking of the first arrivals was graphical and the software identifies the seismic traces to be space-time referenced. Actual picking of the reduced first arrivals was executed by screen digitizing the raw traces *(Appendix 3)*.

This data was later converted to an excel format to increase manipulation. The major steps that were done here are:

1. *Conversion of the *.txt to *.xls format.*
2. *Converting the rational trace numbers to integral numbers (Appendix 5).*
3. *Choosing offset values for each trace.*
4. *Adding the picked reduced first arrival times with the times obtained using equation 6.1 so as to have the actual arrival times (Appendix 4).*

6.2.2. Shot leveling convention.

The software Gremix has a certain configuration which it would attain its shot-geophone nomenclature *(Fig 6.9)*. It recognizes the far end shots (C & D), end shots (A& B), and center shots (E) based on the offset data we feed it.

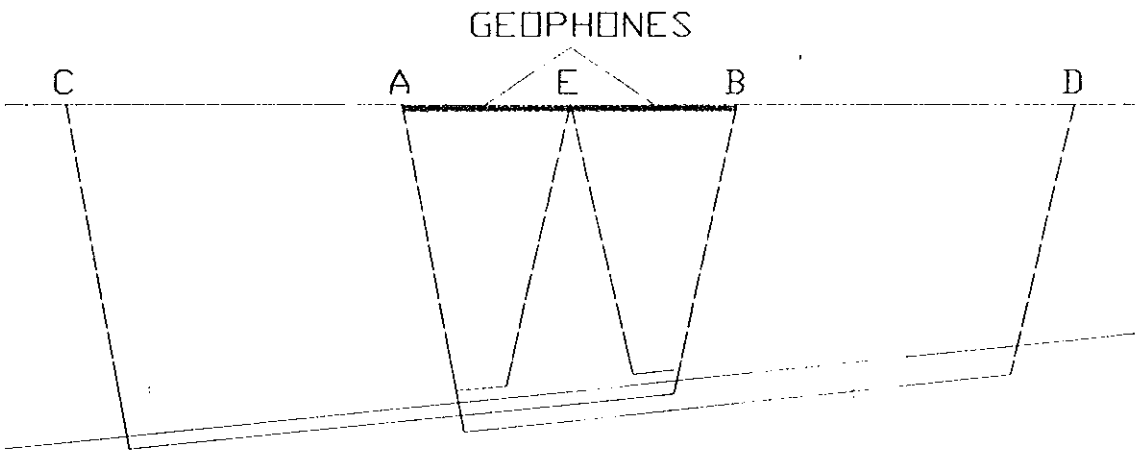

Fig.6.9. GRM shot leveling convention

When a reference position with a value zero is given, the inverting software "Gremix" automatically assigns positive value to the geophones on the right of this relative position and negative values to the left *(Table. 6.1)*. Shot point (SP) 25 the left end shot designed by the letter "A" was assigned to be the reference shot in this study hence, there are negative values that have been recognized as offsets *(Appendix 2)*.

SP	**24**	***25**	**26**	**27**	**28**
Position	-36.9588	0	19.10714	45.93772	107.8622
Offset (km)	-74.478	0	38.504	92.572	217.36
Elevation (m)	1602	1236	953	898	555
Geophone-Spacing (km) for the selected geophones for this particular work 2.015163					

*Indicates the reference shot

Table 6.1. Shot points: position, elevation, and offset, and geophone spacing.

6.2.3. Geophysical Data inversion

Seismic refraction surveys are usually interpreted in terms of the idealized layered structures that the geophone spread is situated on a plane observation surface. In nature, however, the land surface is somewhat irregular, so that the geophones and source points are actually at different elevations. Therefore, the observed arrival times must be adjusted to obtain values that would be expected were the geophones and source points on a plane surface. These time adjustments are called *static corrections*.

In this work, after feeding the data into the processing software Gremix, which is interpretation software, incorporating the methods of the GRM *(Sec. 4.3),* it automatically performs static correction based on the elevation parameters of each geophone *(Fig. 6.10).*

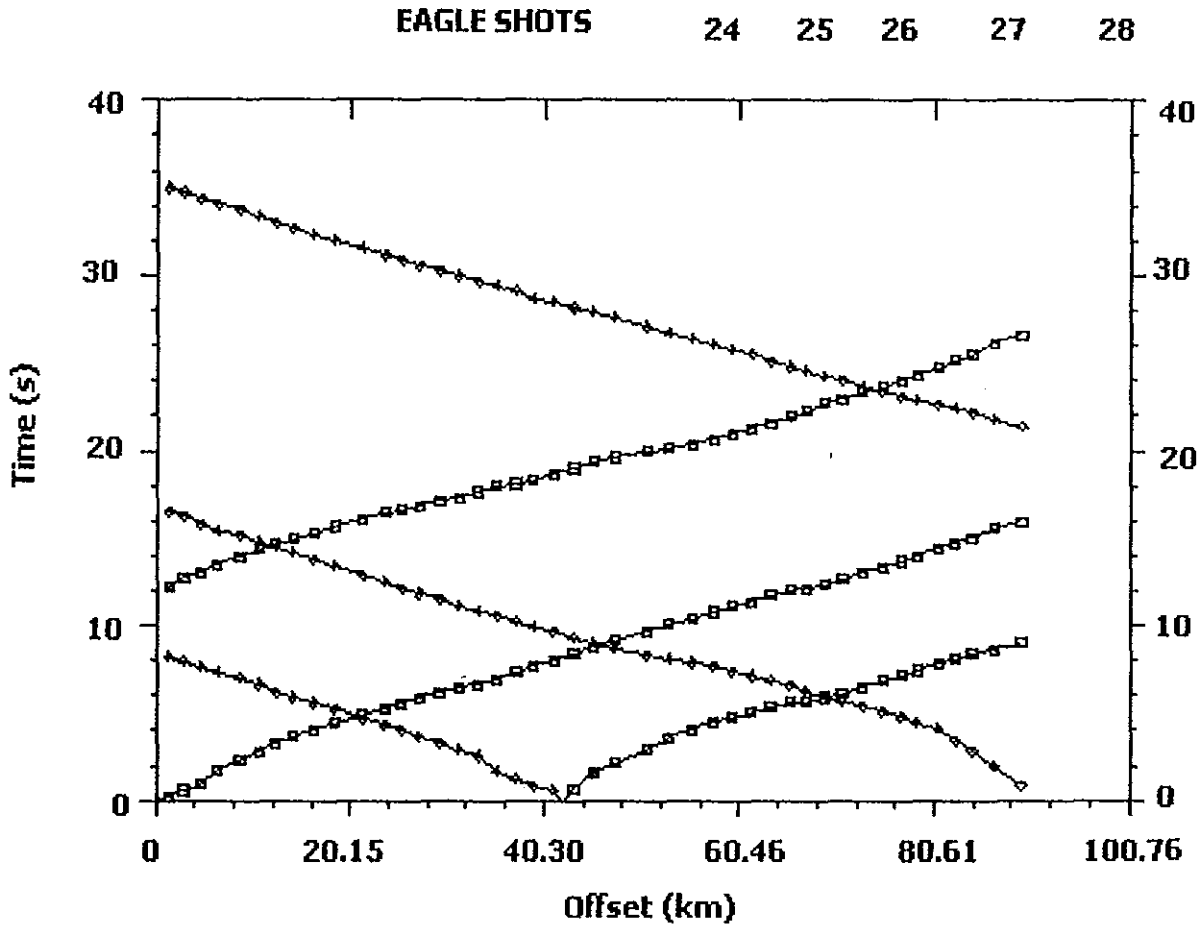

Fig. 6.10. Static corrected arrival times.

6.2.4. Identification of velocity changes.

Reciprocal times were checked before the inversion process is carried out. The inversion process was carried out using Gremix. Optimum XY values were determined for each velocity analysis and time depth function. The time depths were later converted into actual depth with assignment of the true velocity to each layer.

The layer assignments shown in figure 6.11 were:

- Three refractors each from SP 25 & SP 27, indicating the presence of four layers.
- One refractor each from SP 24 & SP 28, indicating the presence of two layers. These layers would be three and four for the shots were beyond the end shots.
- Two refractors were identified for SP 26 on either side of the travel time curve, indicating three layers.

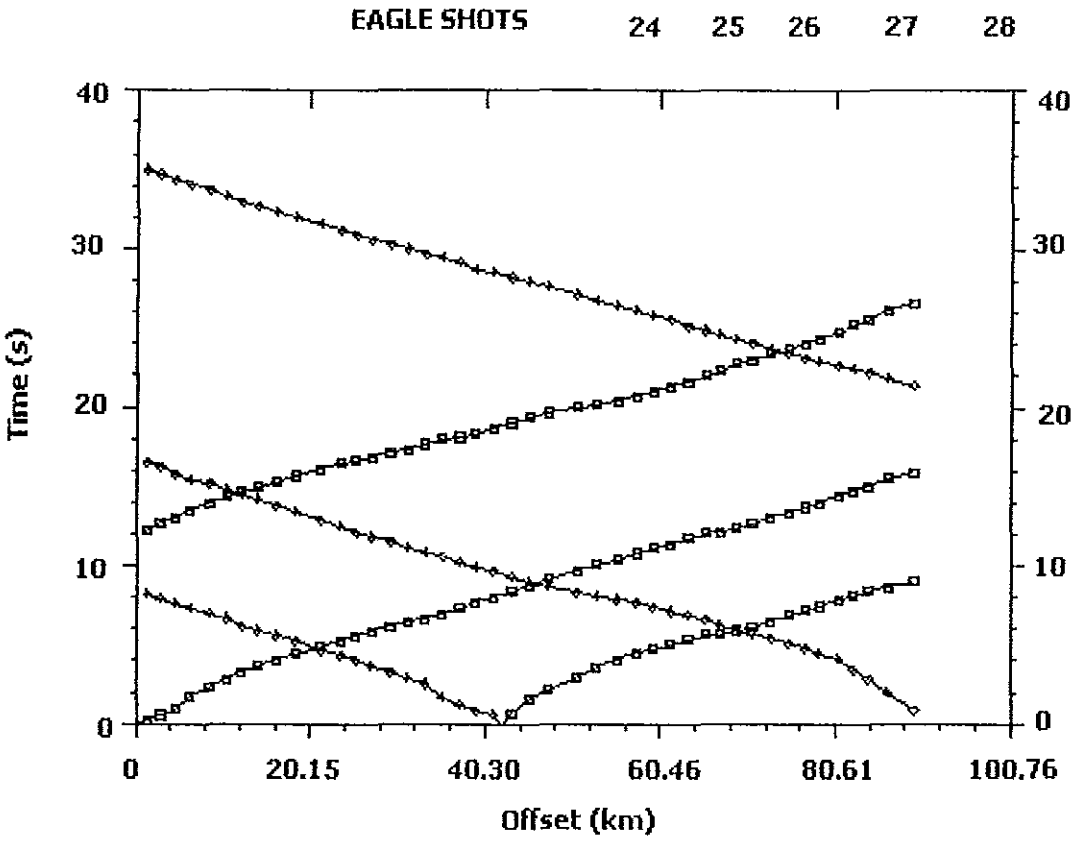

Fig. 6.11. Assigned arrival curves.

The seismic model of the MER using the GRM method of inversion was then finally produced. The output from the inversion software indicates four layers with the maximum depth of 10 km.

7. INTERPRETATION

7.1. Geophysical interpretation

After inverting the data, the geo-seismic model obtained shows four layers of different acoustic property. The seismic velocity distribution of the layers shows little or no lateral variations in the upper two layers. But the third layer exhibits an increase in velocity going from the southwest to the northeast direction *(Fig. 7.1).*

The upper layer with a velocity of 2875 m/s has a more or less constant thickness in the studied area. It generally follows the surface topography and dips northeast along the Main Ethiopian Rift. The lower layers with velocities of 4000 m/s, 5700 m/s and 6400 m/s show undulating refractor surfaces due probably to tectonic forces acting on the region *(Fig 7.1)*

The above geophysical interpretations agree well with the earlier works *(G. Randy Keller, Tadesse, K. et. al., 2004; Mehari Melak, 2004; K. Keranen, S.L. Klemperer et. al., 2004; G.D. Mckenzie et. al., 2004; Maguire, P.K.H, Amha, M., Asfaw, L., Mammo, T.,et. al.., et al., 2004).*

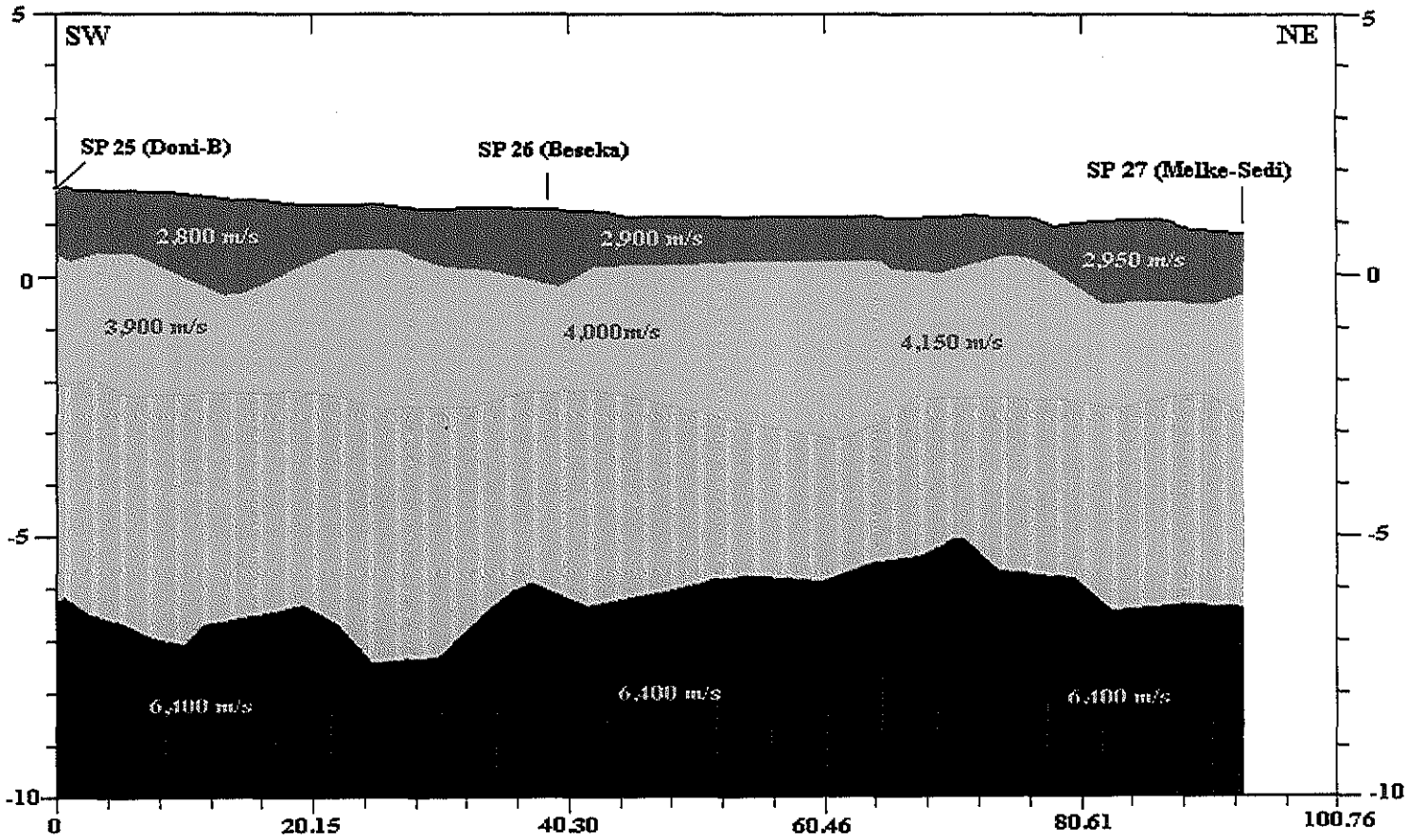

Fig. 7.2 The Geophysical seismic model of the study area.

7.2. Geological interpretation

The geology of the northern Main Ethiopian Rift characterized by the Cenozoic era on top where it is divided into primarily the Miocene-volcanics underlain by Oligocene pre-rift flood volcanics. The experimental seismic velocity of this formation varies from about 1000m/s to 6500m/s.

The Cenozoic era is underlain by the Mesozoic era, which are of considerable thickness where the major lithologies in this period are limestone & sand stones. The experimental determined P-wave velocities in rocks of this period vary from about 1500 m/s to 6000 m/s.

Beneath all the formation lies the basement complex on which all known rock types rest. They are formed under high pressure and temperature giving them a higher density as compared to the other rock types. The experimental P-wave velocities in this complex vary from about 3000 m/s to 7000 m/s, *(Appendix - 6).*

Knowing the geological setting of the study area coupled with the experimentally determined seismic velocities *(Appendix 6),* the geological section interpreted is shown in the figure 7.2.

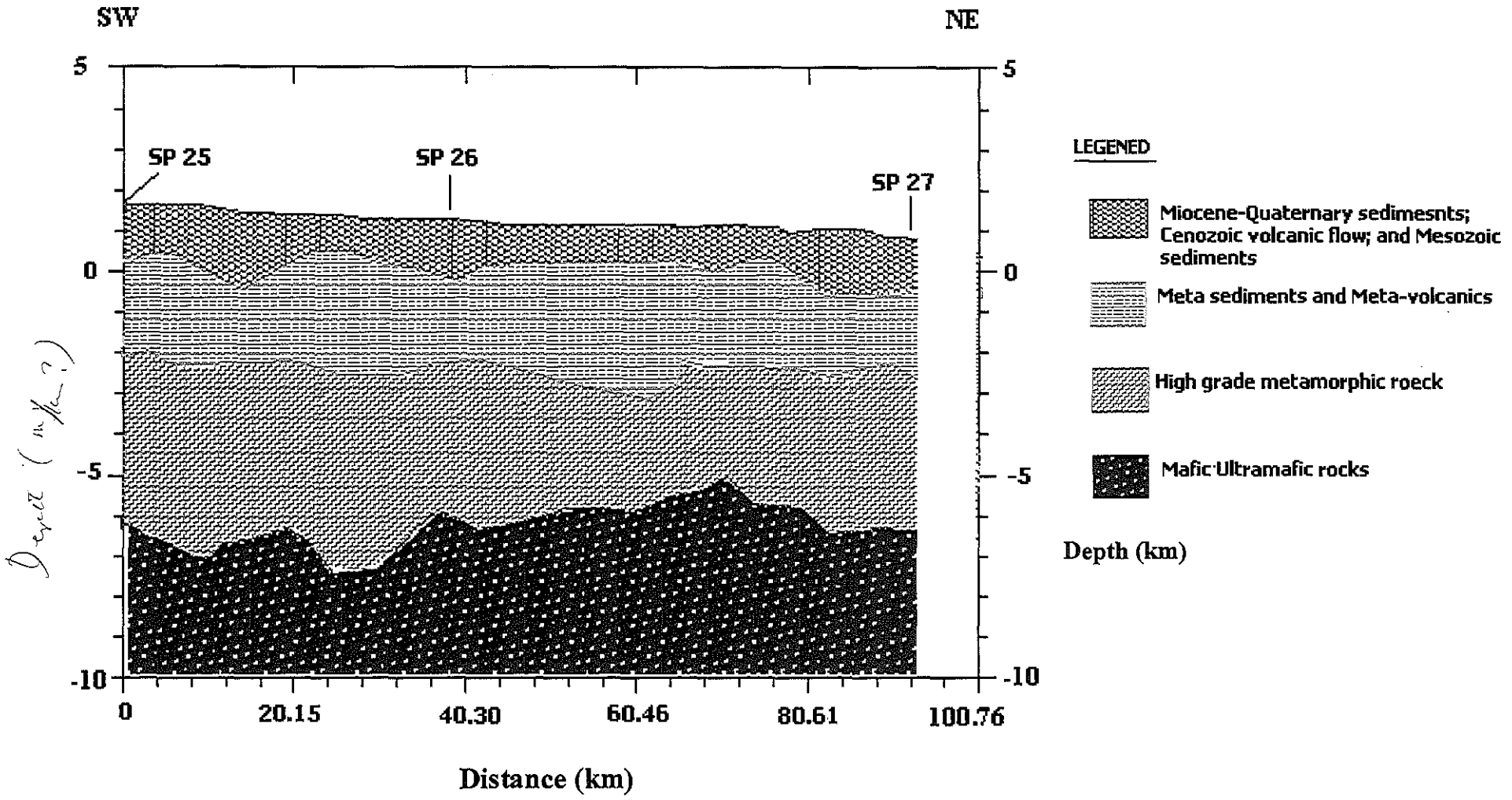

Fig. 7.2 The geological model of the northern Main Ethiopian Rift.

The first layer with an average velocity of 2875 m/s and average thickness of about 2 km is comprised of the Miocene-quaternary sediments, Cenozoic volcanics and the underlain by the Mesozoic sediments.

The second layer therefore is the basement complex as deduced from geophysical and geological evidences. This layer has an average thickness of 2.5 km with an average velocity of 4000 m/s. With regard to the basement complex; the relatively low velocity recorded from this layer could most likely represent low-grade metamorphosed rock mainly composed of meta-sediments and or volcanics.

The third layer has been recognized to be the crystalline basement complex with an average velocity of 5,700m/s. This high velocity could be attributed to the high-grade metamorphic rocks such as gneiss. The depth to the top of this layer is 4.5 km from the surface. This layer has a thickness of about 4 km.

The fourth layer shows typical crustal velocities of more than 6000 m/s. This layer starts at an approximate depth of 8.5km from the surface. Though this layer most likely represents rocks of mafic and ultramafic nature, there is no concrete evidence *(Fig 7.2)*.

The above geological interpretations agree well with the earlier works *(Gidy Wldegebriel et al., 1990; Benvenuti et al., 2002; Di Paola, 1972; T. Chernet & W.K.Hart, 1999; Woldegabriel et al., 1999; M. Bocaletti et al., 1999; K.Keranen et al., 2004).*

8. CONCLUSION AND SUGGESTIONS

8.1. Conclusions

From the results obtained in this study the following conclusions can be made:

Cable-less recordings Texans have been found very effective in carrying out seismic experiments of this scale.

The technique that was used to determine the break points during layer assignments has produced very good results.

Though the data quality is very high with very good energy propagation across the entire length of the profile, the uneven explosive distribution inside the boreholes has caused a slight problem in adjusting amplitude gain when performing data processing.

The study indicates the presence of four layers beneath the northern MER down to a maximum depth of 10 kilometers. These layers from top to bottom have average velocities of 2875 m/s, 4000 m/s, 5700m/s and 6400 m/s at depth of 2 km, 4.5 km, and 8.5 km.

My interpretation shows that, by correlation with the known geology and using deterministic P-wave velocities, the first layer comprises the Miocene-Quaternary sediments, Cenozoic volcanics and sediments of the Mesozoic sequences. The second and third layers on the other hand are Meta-volcanics and Meta-sediments, and high-grade metamorphic rocks respectively. The fourth layer shows typical crustal velocities greater than 6000 m/s. This layer could most likely to be interpreted as comprised of the mafic–ultra mafic rocks.

8.2. Recommendations

Even though, this geophysical study based on refraction seismic methods to the study area is not the first of its kind this work is just a beginning for further detailed studies; therefore further refinements to this work can be made. Based on the out come of this study, I recommend the following:

1. To differentiate between the different flows of volcanic units and isolate the Quaternary sediments, as well as to map the structural features, finer sampling of wave field is needed.

2. Gravity surveying should be carried out to constrain seismic inversion results.

3. Reflection seismic methods should be employed to differentiate between Cenozoic volcanics and the Mesozoic sediments and identify deep-seated structures.

REFERENCES:

1. Alan E. Musset and M. Aftab Khan, 2000, Looking into the earth: *An introduction to geological geophysics*, Cambridge University Press, Cambridge, Great Britain.
2. Berckhemer et al., Ruegg, 1975, *Deep Seismic sounding in the Afar region.*
3. Dobrin M.B., 1976, *Introduction to Geophysical prospecting 3rd edition*, McGraw-Hill book company New York
4. Eagle phase III; *The controlled source seismic project, June 2003, Fieldwork report.*
5. E Daly, D Keir, A. Ayele et al., 2004, *Crustal structure of the northern Main Ethiopian Rift from a tomographic inversion of local earthquakes.*
6. G.D. Macekanzie, et al.., 2004, *Evidence for crustal structures influence on the evolution of the Main Ethiopian Rift.*
7. G.M.Di Paola, 1972, *The Ethiopian rift valley (Between 7^0 00' and $8^0$40 lat North)*: Bulletin Volcanologique, p517-560.
8. G. Woldegabriel et al ....1999, *Temporal relations and geochemical features of felsic volcanism in the central sector of the Main Ethiopian Rift*: Acta Vulcanologica- Vol. 11(1) p.53-67.
9. H. Tesfaye, 2004, *Velocity Structure of the Upper Crust Beneath the Eastern Plateau*, Addis Ababa University

10. I.D. Bastow, G.W. Stuart, Ayele, A. et al., 2004.*Upper Mantel Seismic Structure of Northern Ethiopian Main Rift a Region of Incipient Continental Breakup*

11. K. Karanen, S.L Klemperer et al., 2004, *3D seismic Imaging of a proto-ridge axis in the Main Ethiopian Rift, the east African Rift system: Geodynamics, Resources and Environment.*

12. Magurie, P.K, H, Amha, M., Asfaw, L., Mammo, T., 2004. *EAGLE- The controlled source seismic project.*

13. M. Boccaletti, et al.... 1999, *Pliocene-Quaternary volcanism and faulting the northern main Ethiopian Rift (with two geological maps at scale 1:50,000)*: Acta Vulcanologica – Vol.11 (1) P.83-97.

14. Mehari Melak, 2004, *Velocity structure of the upper crust across the Main Ethiopian Rift.* Addis Ababa University.

15. Paul A. Mohr, 1971, *The Geology of Ethiopia*

16. Palmer, D., 1981. *An introduction to the generalized reciprocal method of seismic refraction interpretation: Geophysics*, 46, 1508-1518.

17. Palmer, D., February 2003, *Application of amplitude in shallow seismic refraction inversion*: A SEG 16th Geophysical conference and exhibition, Adelaide.

18. Robert S. Carmichael, 1989 *Physical properties of rocks and minerals*, CRC press Inc. Florida, United States.

19. Robert W. Lankston, 1989. *The seismic refraction method*: A viable tool for mapping shallow targets into the 1990s: Geophysics, 1535-1542.

20. Robinson, E.S., & Coruh, C., 1988, *Basic Exploration Geophysics*, John Wiley & Sons, Newyork.

21. T. Chernet, W.K.Hart, 1999, *Petrology and geochemistry of volcanism in the northern main Ethiopian Rift-Southern Afar transgression region*: Acta Vulcanologica-Vol.11 (1) p.21-41..

22. Telford, W.B, 1978. *Applied Geophysics*, Cambridge University Press, Cambridge, Great Britain.

23. V. Kazmin, 1972, *Geology of Ethiopia (Explanatory note to the geological map of Ethiopia 1:2,000,000).*

24. V.Kazmin, May 1979, *Stratigraphic and correlation of volcanic rocks in Ethiopia.*

25. William Lowrie, 1997, *Fundamentals of Geophysics*, Cambridge University Press, Cambridge, Great Britain.

APPENDICES

APPENDIX- 1: GEOPHONE STATION, LOCATION, AND ELEVATION

		UTM Location (Adindan)			
Station Location	***Instrument***	***Easting***	***No thing***	***Zone***	***Elevation***
2240	10213	567739	942251.6	37P	1231.8
2241	10824	569088	942435.2	37P	1226.9
2242	10822	569959	942967.7	37P	1217.15
2243	10826	570825	943593.3	37P	1222.2
2244	10821	571527	944323.7	37P	1221.35
2245	10820	572099	945181.2	37P	1214.7
2246	10817	572431	946018.9	37P	1211.9
2247	10814	573323	946632.2	37P	1205
2248	10813	574456	947357.1	37P	1199.75
2249	10812	575267	947727.9	37P	1193.6
2250	10811	576114	948310.1	37P	1195.15
2251	10810	576513	949393.5	37P	1196.25
2252	10809	576707	950390.8	37P	1187.7
2253	10808	577447	951100.5	37P	1185.05
2254	10807	578180	951692.6	37P	1181.45
2255	10806	578640	952489.2	37P	1178.6
2256	10499	579439	953395	37P	1175.9
2257	10497	580269	953944.7	37P	1172.45
2258	10550	581134	954599.1	37P	1171

2259	10549	582113	955142	37P	1161.65
2261	10168	583452	956409	37P	1156.8
2262	10500	584050	957250.8	37P	1140.25
2263	10167	585134	957718.9	37P	1140.2
2264	10165	586040	958601.4	37P	1135.45
2265	10164	586075	959521.8	37P	1132.2
2266	10163	586820	960306.7	37P	1130.25
2267	10162	588004	960662.1	37P	1125
2268	11151	588152	961532.8	37P	1141.6
2269	11150	588976	962330.5	37P	1123.15
2270	11149	589606	963082	37P	1110.9
2271	11145	590157	963948.6	37P	1101.9
2272	11144	590657	964826	37P	1094.95
2273	11143	591221	965650.3	37P	1080.3
2274	11142	591978	966373.5	37P	1057.65
2275	11141	592661	967058.2	37P	1027.75
2276	11140	593246	967846.5	37P	1009.65
2277	11139	593846	968659.4	37P	996.8
2278	11138	594441	969519.3	37P	991.45
2279	11136	591496	973187.4	37P	962.5
2280	11135	591865	974205.9	37P	959.4
2281	11134	592403	974980.1	37P	953.6
2282	10137	591007	977342.6	37P	957
2283	10142	591068	978556.7	37P	967.35

2284	10141	591385	979634.6	37P	982.55
2285	10140	591790	980487.6	37P	976.35
2286	10145	592306	981459.5	37P	978.4
2287	10144	592652	982490.1	37P	977.5
2288	10143	592599	983860.2	37P	966.5
2289	10148	592773	985135.2	37P	962.75
2291	10032	592620	987646.7	37P	985.8
2292	10031	592406	988908.7	37P	990.55
2293	10036	592283	990404.8	37P	996.5
2294	10035	592071	991863.3	37P	999.2
2295	10034	591886	993241.5	37P	999.65
2296	10597	591997	994426.4	37P	994.1
2297	10605	592223	995441	37P	995.2
2298	10594	592791	996301.8	37P	1012.15
2299	10959	593737	996934	37P	1039.5
2300	10962	594375	997649.9	37P	1042.65
2301	10958	594788	998647.7	37P	1036.9
2302	10965	595004	999554.2	37P	1029.7
2303	10971	595676	1000419	37P	1030.05
2304	10980	596197	1001347	37P	1042.3
2305	10976	596518	1002212	37P	1052.05
2306	10967	598225	1002175	37P	987.95
2307	10964	599270	1002711	37P	962.05
2308	10961	599739	1003647	37P	932.15

2309	10975	601528	1003672	37P	870.6
2310	10966	602044	1004330	37P	833.1
2311	10963	602352	1005316	37P	817.95
2312	10960	602607	1006529	37P	799.95
2313	10957	602856	1007497	37P	793.95
2314	10077	603553	1008278	37P	789.45
2315	10080	604147	1009147	37P	796.35
2316	10076	604405	1010099	37P	802.1
2317	10083	606077	1010172	37P	792.5
2318	10079	606210	1011090	37P	792.25
2319	10086	608251	1010890	37P	778.3
2320	10082	608487	1012057	37P	778.05
2321	10491	609848	1012455	37P	770
2322	11192	611980	1012008	37P	763.05
2323	11193	613731	1012058	37P	760.4
2324	11188	614688	1012112	37P	759.2
2325	11189	616026	1012592	37P	754.5
2326	11190	617107	1012862	37P	752.95
2327	11185	618766	1013514	37P	751.6

APPENDIX - 2: OFFSETS OF GEOPHONES FROM EACH SHOT

	Offsets of geophones from each shots				
Trace #	***SP24***	***SP25***	***SP26***	***SP27***	***SP28***
		SHOT 25			
220	71.972	1.245	-42.2	-92.35	-217.413
221	72.972	1.913	-41.246	-91.394	-216.508
222	73.981	2.8	-40.233	-90.377	-215.533
223	74.878	3.663	-39.228	-89.371	-214.548
224	75.695	4.525	-38.198	-88.341	-213.519
225	76.292	5.24	-37.322	-87.468	-212.624
226	77.337	6.321	-36.3	-86.442	-211.645
227	78.649	7.667	-35.051	-85.183	-210.448
228	79.54	8.551	-34.284	-84.402	-209.721
229	80.536	9.579	-33.326	-83.432	-208.794
230	81.284	10.519	-32.208	-82.325	-207.658
231	81.827	11.292	-31.274	-81.404	-206.694
232	82.771	12.312	-30.271	-80.396	-205.712
233	83.675	13.257	-29.367	-79.482	-204.832
234	84.402	14.127	-28.448	-78.567	-203.911
235	85.488	15.329	-27.249	-77.362	-202.727
236	86.461	16.31	-26.335	-76.431	-201.841
237	87.515	17.394	-25.317	-75.393	-200.845
238	88.628	18.49	-24.342	-74.382	-199.891

239	90.359	20.333	-22.572	-72.574	-198.131
240	91.249	21.342	-21.541	-71.537	-197.102
241	92.424	22.462	-20.618	-70.538	-196.171
242	93.615	23.73	-19.418	-69.294	-194.957
243	94.021	24.362	-18.583	-68.518	-194.136
244	95.027	25.444	-17.544	-67.447	-193.087
245	96.256	26.566	-16.723	-66.484	-192.205
246	96.749	27.252	-15.869	-65.684	-191.373
247	97.835	28.399	-14.811	-64.561	-190.278
248	98.731	29.376	-13.878	-63.583	-189.315
249	99.601	30.368	-12.874	-62.557	-188.292
250	100.439	31.339	-11.877	-61.547	-187.279
251	101.306	32.314	-10.916	-60.551	-186.288
252	102.307	33.361	-10.007	-59.528	-185.292
253	103.223	34.327	-9.179	-58.58	-184.366
254	104.098	35.294	-8.296	-57.601	-183.396
255	105.006	36.295	-7.409	-56.59	-182.394
256	105.928	37.321	-6.513	-55.546	-181.357
257	105.112	38.12	-4.21	-54.3	-179.558
258	105.947	39.155	-3.286	-53.27	-178.487
259	106.803	40.096	-2.435	-52.33	-177.549
260	106.846	41.208	-3.821	-51.418	-176.191
261	107.549	42.256	-4.339	-50.473	-175.111
			SHOT 26		

262	108.4	43.333	4.829	-49.466	-174.021
263	109.207	44.271	5.27	-48.566	-173.08
264	110.172	45.368	5.896	-47.506	-171.981
265	111.026	46.421	6.752	-46.529	-170.921
266	111.756	47.563	8.085	-45.592	-169.769
267	112.626	48.748	9.291	-44.581	-168.585
268	113.965	50.858	11.789	-43.003	-166.516
269	114.535	51.862	13.071	-42.358	-165.558
270	115.344	53.137	14.567	-41.512	-164.349
271	116.066	54.345	16.041	-40.807	-163.229
272	116.77	55.503	17.432	-40.171	-162.171
273	117.595	56.621	18.589	-39.427	-161.118
274	118.412	57.638	19.566	-38.691	-160.142
275	119.398	58.659	20.362	-37.756	-159.11
276	120.53	59.634	20.932	-36.62	-158.064
277	121.476	60.554	21.631	-35.707	-157.118
278	122.432	61.635	22.63	-34.847	-156.053
279	123.179	62.546	23.539	-34.218	-155.175
280	124.247	63.615	24.424	-33.221	-154.085
281	125.247	64.679	25.379	-32.331	-153.021
282	126.048	65.597	26.265	-31.666	-152.123
283	127.336	66.326	26.408	-30.143	-151.222
284	128.479	67.28	27.098	-28.971	-150.211
285	129.44	68.328	28.104	-28.135	-149.168

286	130.835	69.199	28.51	-26.519	-148.194
287	131.65	70.024	29.275	-25.763	-147.364
288	132.514	71.034	30.306	-25.062	-146.366
289	133.485	72.218	31.543	-24.347	-145.204
290	134.301	73.188	32.543	-23.76	-144.251
291	135.342	74.21	33.481	-22.834	-143.216
292	136.356	75.256	34.478	-21.998	-142.166
293	137.174	76.216	35.464	-21.477	-141.221
294	138.491	77.091	36.032	-19.85	-140.274
295	139.185	77.954	36.944	-19.484	-139.426
296	140.616	78.804	37.451	-17.561	-138.529
297	141.55	79.929	38.624	-17.038	-137.408
298	142.848	80.968	39.502	-15.622	-136.364
299	144.204	81.713	39.971	-13.663	-135.67
300	145.59	82.707	40.806	-11.98	-134.763
301	146.369	83.284	41.311	-11.057	-134.249
302	147.715	84.437	42.392	-9.634	-133.183
303	148.725	85.272	43.175	-8.531	-132.435
304	150.44	86.772	44.616	-6.739	-131.075
305	151.958	88.066	45.863	-5.108	-129.946
306	153.816	89.652	47.408	-3.113	-128.598
307	155.706	91.383	49.12	-1.189	-127.065
				SHOT 27	

APPENDIX-3: THE RAW PICKED FIRST ARRIVALS OF SHOT 24

Trace #	*Reduced time*	
220.035	0.227	1
222.159	0.364	1
224.071	0.424	1
225.982	0.621	1
228.106	0.667	1
229.911	0.758	1
232.035	0.833	1
234.265	0.864	1
235.858	0.864	1
237.982	0.879	1
240	0.864	1
242.23	0.833	1
243.823	0.788	1
245.841	0.742	1
248.177	0.667	1
250.089	0.561	1
252.212	0.591	1
253.911	0.621	1
256.142	0.591	1
257.947	0.667	1
260.177	0.848	1

262.089	0.939	1
264.212	0.985	1
266.018	1	1
267.929	0.955	1
270.053	0.879	1
271.965	0.848	1
273.982	0.879	1
276	0.864	1
278.124	0.879	1
280.035	0.864	1
281.841	0.894	1
284.071	0.848	1
285.982	0.879	1
288	0.864	1
290.124	0.939	1
291.929	0.879	1
294.159	0.909	1
295.965	0.864	1
298.195	0.894	1
300.106	0.909	1
302.018	0.879	1
303.929	1.045	1
305.947	0.985	1

244	25.444	12.6262739	1135.45	15604.3	8065.53	6503.75	17726.6	31971.8
246	27.252	13.5234718	1130.25	15886.2	8495.23	5977.6	17395.4	31646.1
248	29.376	14.5774808	1141.6	16168	8924.93	5202.06	17064.1	31320.3
250	31.339	15.5515956	1110.9	16449.8	9354.63	4426.52	16732.9	30994.6
252	33.361	16.5549884	1094.95	16731.6	9784.33	3650.98	16401.6	30668.9
254	35.294	17.514216	1057.65	17013.5	10214	2875.45	16070.4	30343.2
256	37.321	18.5200899	1009.65	17295.3	10643.7	2099.91	15739.2	30017.5
258	39.155	19.43019	991.45	17577.1	11073.4	1324.37	15407.9	29691.8
260	41.208	20.4489662	959.4	17859	11503.1	548.833	15076.7	29366.1
262	43.333	21.5034714	957	18140.8	11932.8	1198.83	14745.4	29021.2
264	45.368	22.5133153	982.55	18422.6	12362.5	2024.16	14339.2	28676.3
266	47.563	23.6025572	978.4	18751.1	12728.6	2849.48	13932.9	28331.4
268	50.858	25.2376607	966.5	19079.5	13094.6	3674.81	13526.6	27986.5
270	53.137	26.3685866	978.8	19407.9	13460.7	4500.13	13120.3	27641.5
272	55.503	27.5426851	990.55	19736.3	13826.8	5325.46	12714	27296.6
274	57.638	28.6021528	999.2	20064.7	14192.8	6150.78	12307.7	26951.7

276	59.634	29.5926434	994.1	20393.2	14558.9	6976.11	11901.4	26606.8
278	61.635	30.5856152	1012.15	20721.6	14924.9	7339.7	11495.1	26261.9
280	63.615	31.568166	1042.65	21050	15291	7703.29	11088.8	25916.9
282	65.597	32.5517092	1029.7	21378.4	15657	8066.89	10682.5	25572
284	67.28	33.3868774	1042.3	21706.8	16023.1	8430.48	10276.2	25227.1
286	69.199	34.3391577	987.95	22035.3	16389.1	8794.08	9489.75	24882.2
288	71.034	35.249754	932.15	22363.7	16712.4	9157.67	8703.26	24537.3
290	73.188	36.3186502	833.1	22692.1	17035.6	9521.26	7916.77	24192.3
292	75.256	37.3448699	799.95	23020.5	17358.8	9831.67	7130.28	23847.4
294	77.091	38.2554662	789.45	23348.9	17682	10142.1	6343.78	23502.5
296	78.804	39.1055215	802.1	23677.3	18005.2	10452.5	5557.29	23157.6
298	80.968	40.17938	792.25	24005.8	18328.4	10762.9	4770.8	22812.7
300	82.707	41.0423375	778.05	24334.2	18651.6	11073.3	3984.31	22467.8
302	84.437	41.9008289	763.05	24662.6	18974.9	11383.7	3197.82	22122.8
304	86.772	43.0595441	759.2	24991	19298.1	11694.1	2411.32	21777.9
306	89.652	44.4887089	752.95	25319.4	19621.3	12004.6	1624.83	21433

APPENDIX - 5: PICKED FIRST ARRIVALS OF EACH SHOT WITH THEIR GEOPHONE OFF

	SHOT 24		*SHOT 25*		*SHOT 26*		*SHOT 27*		*SHOT 28*	
Trace #	*Offset*	*First arrivals*	*Offset*	*First arrivals*	*Offset*	*First arrivals*	*Offset*	*First arrivals*	*Offset*	*First arrivals*
220	71.972	0.227	1.245	-0.848	-42.2	1.212	-92.35	1.167	-217.41	-1.212
221	72.972		1.913		-41.246		-91.394		-216.51	
222	73.981	0.364	2.8	-0.227	-40.233	1.242	-90.377	1.136	-215.53	-1.212
223	74.878		3.663		-39.228		-89.371		-214.55	
224	75.695	0.424	4.525	0.136	-38.198	1.258	-88.341	1.03	-213.52	-1.227
225	76.292		5.24		-37.322		-87.468		-212.62	
226	77.337	0.621	6.321	0.712	-36.3	1.258	-86.442	1.015	-211.65	-1.212
227	78.649		7.667		-35.051		-85.183		-210.45	
228	79.54	0.667	8.551	0.848	-34.284	1.288	-84.402	1.061	-209.72	-1.197
229	80.536		9.579		-33.326		-83.432		-208.79	
230	81.284	0.758	10.519	1.076	-32.208	1.303	-82.325	1.03	-207.66	-1.242
231	81.827		11.292		-31.274		-81.404		-206.69	
232	82.771	0.833	12.312	1.227	-30.271	1.121	-80.396	1.061	-205.71	-1.273

233	83.675		13.257		-29.367		-79.482		-204.83	
234	84.402	0.864	14.127	1.318	-28.448	1.152	-78.567	1.061	-203.91	-1.318
235	85.488		15.329		-27.249		-77.362		-202.73	
236	86.461	0.864	16.31	1.318	-26.335	1.197	-76.431	1.061	-201.84	-1.288
237	87.515		17.394		-25.317		-75.393		-200.85	
238	88.628	0.879	18.49	1.333	-24.342	1.182	-74.382	1.045	-199.89	-1.288
239	90.359		20.333		-22.572		-72.574		-198.13	
240	91.249	0.864	21.342	1.348	-21.541	1.061	-71.537	0.97	-197.1	-1.303
241	92.424		22.462		-20.618		-70.538		-196.17	
242	93.615	0.833	23.73	1.273	-19.418	1.121	-69.294	0.955	-194.96	-1.303
243	94.021		24.362		-18.583		-68.518		-194.14	
244	95.027	0.788	25.444	1.333	-17.544	1.136	-67.447	0.894	-193.09	-1.318
245	96.256		26.566		-16.723		-66.484		-192.21	
246	96.749	0.742	27.252	1.318	-15.869	1.045	-65.684	0.894	-191.37	-1.333
247	97.835		28.399		-14.811		-64.561		-190.28	
248	98.731	0.667	29.376	1.258	-13.878	0.985	-63.583	0.879	-189.32	-1.273
249	99.601		30.368		-12.874		-62.557		-188.29	
250	100.439	0.561	31.339	1.212	-11.877	0.924	-61.547	0.894	-187.28	-1.227

251	101.306		32.314		-10.916		-60.551		-186.29	
252	102.307	0.591	33.361	1.091	-10.007	0.879	-59.528	0.909	-185.29	-1.212
253	103.223		34.327		-9.179		-58.58		-184.37	
254	104.098	0.621	35.294	1.076	-8.296	0.273	-57.601	0.97	-183.4	-1.167
255	105.006		36.295		-7.409		-56.59		-182.39	
256	105.928	0.591	37.321	1.121	-6.513	0.106	-55.546	0.97	-181.36	-1.091
257	105.112		38.12		-4.21		-54.3		-179.56	
258	105.947	0.667	39.155	1.152	-3.286	0.076	-53.27	1.045	-178.49	-1.061
259	106.803		40.096		-2.435		-52.33		-177.55	
260	106.846	0.848	41.208	1.136	-3.821	0.212	-51.418	1.121	-176.19	-0.879
261	107.549		42.256		-4.339		-50.473		-175.11	
262	108.4	0.939	43.333	1.136	4.829	0.394	-49.466	1.076	-174.02	-0.848
263	109.207		44.271		5.27		-48.566		-173.08	
264	110.172	0.985	45.368	1.227	5.896	0.53	-47.506	1.091	-171.98	-0.773
265	111.026		46.421		6.752		-46.529		-170.92	
266	111.756	1	47.563	1.212	8.085	0.758	-45.592	1.121	-169.77	-0.697
267	112.626		48.748		9.291		-44.581		-168.59	
268	113.965	0.955	50.858	1.167	11.789	0.939	-43.003	1.121	-166.52	-0.652

269	114.535		51.862		13.071		-42.358		-165.56	
270	115.344	0.879	53.137	1.197	14.567	1.167	-41.512	1.167	-164.35	-0.697
271	116.066		54.345		16.041		-40.807		-163.23	
272	116.77	0.848	55.503	1.121	17.432	1.152	-40.171	1.182	-162.17	-0.667
273	117.595		56.621		18.589		-39.427		-161.12	
274	118.412	0.879	57.638	1.167	19.566	1.227	-38.691	1.242	-160.14	-0.621
275	119.398		58.659		20.362		-37.756		-159.11	
276	120.53	0.864	59.634	1.167	20.932	1.242	-36.62	1.273	-158.06	-0.591
277	121.476		60.554		21.631		-35.707		-157.12	
278	122.432	0.879	61.635	1.106	22.63	1.273	-34.847	1.318	-156.05	-0.515
279	123.179		62.546		23.539		-34.218		-155.18	
280	124.247	0.864	63.615	1.121	24.424	1.258	-33.221	1.303	-154.09	-0.591
281	125.247		64.679		25.379		-32.331		-153.02	
282	126.048	0.894	65.597	1.091	26.265	1.242	-31.666	1.364	-152.12	-0.545
283	127.336		66.326		26.408		-30.143		-151.22	
284	128.479	0.848	67.28	0.924	27.098	1.152	-28.971	1.409	-150.21	-0.47
285	129.44		68.328		28.104		-28.135		-149.17	
286	130.835	0.879	69.199	0.803	28.51	1.152	-26.519	1.455	-148.19	-0.485

287	131.65		70.024		29.275		-25.763		-147.36	
288	132.514	0.864	71.034	0.833	30.306	1.061	-25.062	1.455	-146.37	-0.394
289	133.485		72.218		31.543		-24.347		-145.2	
290	134.301	0.939	73.188	0.818	32.543	1.045	-23.76	1.455	-144.25	-0.379
291	135.342		74.21		33.481		-22.834		-143.22	
292	136.356	0.879	75.256	0.803	34.478	1.121	-21.998	1.424	-142.17	-0.333
293	137.174		76.216		35.464		-21.477		-141.22	
294	138.491	0.909	77.091	0.818	36.032	1.152	-19.85	1.485	-140.27	-0.288
295	139.185		77.954		36.944		-19.484		-139.43	
296	140.616	0.864	78.804	0.818	37.451	1.182	-17.561	1.47	-138.53	-0.242
297	141.55		79.929		38.624		-17.038		-137.41	
298	142.848	0.894	80.968	0.894	39.502	1.242	-15.622	1.53	-136.36	-0.121
299	144.204		81.713		39.971		-13.663		-135.67	
300	145.59	0.909	82.707	0.909	40.806	1.288	-11.98	1.424	-134.76	-0.045
301	146.369		83.284		41.311		-11.057		-134.25	
302	147.715	0.879	84.437	0.955	42.392	1.288	-9.634	1.182	-133.18	-0.015
303	148.725		85.272		43.175		-8.531		-132.44	
304	150.44	1.045	86.772	1.076	44.616	1.136	-6.739	0.833	-131.08	-0.03

305	151.958		88.066		45.863		-5.108		-129.95	
306	153.816	0.985	89.652	1	47.408	1.106	-3.113	0.318	-128.6	-0.061
307	155.706		91.383		49.12		-1.189		-127.065	

APPENDIX - 6: P - WAVE VELOCITIES IN MATERIALS BODIES.

ROCK TYPE	P-WAVE VELOCITY (m/s)
UNCONSOLIDATED SEDIMENTS	
Clay	1000 – 2500
Sand (dry)	200 –1000
Sand (saturated)	1500 – 2000
SEDIMENTARY ROCKS	
Anhydrite	6000
Chalk	2100 – 4500
Coal	1700 - 4500
Dolomite	4000 – 7000
Limestone	3900 – 6200
Shale	2000 – 5500
Salt	4600
Sandstone	2000 – 5000
IGNEOUS AND METAMORPHIC ROCKS	
Basalt	5300 – 6500
Granite	4700 – 6000
Gabbaro	6500 – 7000
Slate	3500 – 4400
Ultramafic rocks	7500 – 8500
OTHERS	
Air	300

Natural gas	430
Ice	340
Water	1400 – 1530
Oil	1300 – 1400
Soil	100-500
Concrete	3000-3500